Spring 2009

Continuous control of lunar orbits via electric propulsion

Sunil Aggarwal

Department:

CONTINUOUS CONTROL OF LUNAR ORBITS VIA ELECTRIC PROPULSION

by

SUNIL AGGARWAL

A THESIS

Presented to the Faculty of the Graduate School of the

MISSOURI UNIVERSITY OF SCIENCE AND TECHNOLOGY

In Partial Fulfillment of the Requirements for the Degree

MASTER OF SCIENCE IN AEROSPACE ENGINEERING

2009

Approved by

Dr. Henry J. Pernicka, Advisor

Dr. Robert G. Landers

Dr. Joshua L. Rovey

ABSTRACT

To find definite answers for the presence of water on the poles of Moon, to facilitate selection of future lunar landing sites and aid in construction of architectural bases, to assist proper lunar resource utilization and to improve lunar gravity models there is a great interest and need for highly accurate, reliable and efficient lunar surface mapping and communication. This thesis is intended to aid in proper selection of orbits for future lunar missions by demonstrating the impact of using electric propulsion on the search space of feasible and useful lunar orbits. The requirements for future lunar mapping and communication are studied and possible options to meet them are investigated. Based on coverage analysis, a constellation of three satellites in high altitude, circular and polar geo-synchronous orbit is proposed to provide an improved lunar communications architecture compared to those previously recommended in literature. Low altitude, circular and polar Sun-synchronous orbits are found to be the best candidate to meet future lunar mapping needs. The feasibility of using electric propulsion for stationkeeping and providing the orbit plane rotation required by these lunar mapping and communication options is determined.

The perturbations due to the gravitational forces from the Earth, the Sun, and the non-spherical shape of the Moon and due to solar radiation pressure are utilized as a framework for deriving a nonlinear mathematical model that describes the dynamics of spacecraft orbiting the Moon. After converting the nonlinear system model into a linear-like structure, the control inputs required for maintaining spacecraft in desired lunar orbits are found by employing a robust suboptimal control approach based on State Dependent Algebraic Riccati Equation (SDRE) technique. Furthermore, a closed-form solution that provides an analytic expression for the control law is developed. This solution eliminates the need for solving the Riccati equation at each time step, significantly reducing the required online computations and making the implementation of the controller very simple and easy. Various simulations are performed and numerical results obtained are analyzed, to demonstrate the effectiveness of the controller and determine if the required control inputs can be provided by currently available electric propulsion systems.

ACKNOWLEDGMENTS

I would like to thank the Missouri University of Science & Technology for providing me with great opportunities in order to follow the right path to fulfill my dreams. I highly thank and express my sincere gratitude to my advisor Dr. Henry J. Pernicka, who patiently guided and encouraged me throughout my studies. I thank Dr. Robert G. Landers and Dr. Joshua L. Rovey for taking out time from their busy schedule to serve on my committee, providing great suggestions and reviewing my work. I highly appreciate the conversations I had with Dr. S. N. Balakrishnan, Nathan Harl, Suman Sanyal, Daero Lee, and Jie Ding, that helped me a lot in problem solving and understanding various concepts, without which I would have never finished this thesis. I specially thank them all for their time and assistance. I also thank Jeanine Bruening at the MS&T writing center for editing parts of my thesis.

I thank my family and friends for their continuous support and well wishing. I am very grateful to Jennifer D'souza, Saurabh Agarwal, Vikrant Gaur, Shagnik Saha and Santosh Poreddy, who took care of me all this time when I away from home. Finally, I would like to dedicate this thesis to my grandparents Mr. Hari Krishan Aggarwal and Mrs. Prem Lata Aggarwal.

TABLE OF CONTENTS

LIST OF ILLUSTRATIONS

Page

1. INTRODUCTION

Our closest neighbor, the Moon, being a proving ground for a wide range of space operations and processes [1], has always been regarded as the first milestone for continued and sustainable space exploration. A series of Luna (Russian) and Ranger (USA) flyby, probe, and impact missions during late 50s and early 60s were the first to physically explore the Moon and provide lunar topographic, gravity, and environmental data together with high-resolution images of the Moon obtained using TV cameras. These were followed by Surveyor and Lunar Orbiter missions (USA, 1966-1968), which provided extensive coverage of the lunar surface to aid in selection of lunar landing sites for the Apollo missions. The principle task of the Apollo missions was to land humans on the Moon and return them safely to Earth with samples of lunar rock; this was accomplished in 1969. The Apollo missions revolutionized the understanding of the evolution of the solar system. They also discovered irregular mass distribution throughout the Moon with large concentrations of mass below the lunar basins. The Apollo missions had to perform many unplanned orbit corrections because of the unexpected perturbations due to the nonspherical shape of Moon [2, 3].

No spacecraft flew to the Moon for about 25 years after the Russian probe Luna 24 landed on the Moon in 1976. In 1991 and 1992 however, the Galileo spacecraft (USA) flew by the Moon twice on its way to Jupiter, taking high resolution pictures of the Moon at various wavelengths. Later with the help of its laser and radar devices, the Clementine spacecraft (USA) in 1994 found astonishing evidence of frozen water on the poles of the Moon. Clementine also improved lunar gravity models, but no far side tracking was done and the data collected were not very accurate due to the spacecraft's high orbit (semimajor axis, a = 5116 km and eccentricity, e = 0.36). Lunar Prospector (USA, 1998), however, spent more than a year and half near lunar surface in low orbits (< 100 km) collecting valuable gravity and magnetic data, which were tracked for the near side of the Moon. It also found strong evidence for the presence of ice on the lunar poles [3, 4].

Based on the results obtained from the Lunar Prospector mission and with President Bush's support for space exploration, NASA declared its "Global Exploration Strategy" in 2006. This exploration strategy provides a framework of coordination among

14 space agencies throughout the world for sustainable space exploration. It clearly set forth's an action plan for a shared vision for space exploration that aims to build a permanent base on the Moon and carry out robotic and human exploration of Mars and beyond [1]. Four unmanned lunar missions including SMART-1 (Europe), Chang'e (China), SELENE (Japan) and Chandrayaan-1 (India), have already been successfully carried out in the last five years. The Lunar Reconnaissance Orbiter (USA) is scheduled to be launched in spring, 2009 [10, 11]. NASA plans to start building a lunar base on the Moon's south pole no later than 2020. Very little is known about the poles of the Moon; polar temperatures, concentrations of accessible ice, and availability of sunlight for power generation are some of the important factors that must still be explored for proper site selection and mission execution [8, 9].

1.1. CURRENT AND FUTURE REQUIREMENTS FOR LUNAR ORBITS

In order to find definite answers for the presence of water on the poles of Moon, to facilitate selection of future lunar landing sites and aid in construction of architectural bases, to assist proper lunar resource utilization and to improve lunar gravity models there is a great interest and need for highly accurate, reliable and efficient lunar surface mapping and communication [1, 3, 4, 20].

The major technical challenge for operating at the Lunar South Pole (Aitken Basin and Shackleton Crater) which is the proposed area for a lunar base is that the Earth is not usually visible for direct radio communications [27]. Also, present Earth-based lunar communication capabilities support operations in the Earth facing side, i.e., near side of the Moon. Thus, in order to cover far side operations such as far side gravity mapping and Lunar Astronomical Observatory; it is essential to have a communication relay satellite system [16]. These lunar communication and navigation systems need to provide continuous South Pole coverage to support the robotic and human exploration activities essential to build the lunar base. They need to later evolve into a global coverage system that provides a high navigational accuracy to support the permanent lunar base [25, 28].

Lunar mapping orbits require the spacecraft's orbit to be of low altitude (< 100 km) for high resolution and precision; near circular eccentricity ($e \approx 0$) and near polar

inclination ($85 \le i \le 95$ deg) for adjacent orbital passes with significant overlapping and global coverage at all latitudes; and near Sun-synchronous orientation for consistent illumination and efficient imaging [21]. Sun-synchronous orbits rotate at the same rate at which the orbiter's center body revolves around the Sun, such that the orbit plane is always oriented at a constant angle with a vector directed from the Sun to the body the spacecraft is orbiting (see Figure 1.1). This provides a constant surface illumination or Sun angle, which is highly desired by astronomers for imaging and other experiments that capture light reflected by the center body.

Sun-synchronous orbits have long been the ideal choice for mapping. Past and present Sun-synchronous Earth orbiters [13] include Radarsat, Aqua, Terra, Aura, CloudSat, Aquarius, NIMBUS, LANDSAT, SME and more, but no spacecraft has ever been placed in a Sun-synchronous lunar orbit. Sun-synchronous Earth orbiters benefit from the change in ascending node due to the high J_2 value (0.00108263), i.e., the

Figure 1.1 Synchronous Orbits

oblateness or equatorial bulge of Earth. The equation describing the rate of change in the ascending node, $\dot{\Omega}$ due to equatorial bulge is expressed as

$$\dot{\Omega} = -\frac{3}{2} J_2 \, n \left[\frac{R}{a(1-e^2)} \right]^2 \cos(i) \tag{1-1}$$

where n is mean motion given by $n = \sqrt{Gm / a^3}$ and *a, e,* and *i* are three of the six classical elements (semimajor axis, eccentricity and inclination respectively) that describe the orbit of the satellite. The terms *R* and *m* are the radius and mass of the center body respectively and *G* is the universal gravitational constant. Earth and the Moon make one complete revolution about the Sun in one year, therefore, to obtain an exact Sun synchronous orbit, the rate of change of ascending node needs to be $\dot{\Omega} = (360)/(365.26) = 0.9856 \text{ deg per day}$ as measured relative to an inertial frame. For Earth orbiters, this rate of change ascending node can easily be obtained by choosing a combination of certain acceptable values of *a, e,* and *i*. However, for lunar orbiters this cannot be done because of Moon's lower J_2. The J_2 of the Moon (0.00020433) is very small and thus a Sun-synchronous Moon orbiter requires extra control in order to maintain a Sun-synchronous trajectory.

The Moon has no atmosphere, which means it offers no drag or heating of spacecraft in low orbits; thus lunar orbits can be very low. Lunar Prospector spent six months orbiting only 30 km above the lunar surface. However, the problem is the non-uniform shape of Moon and the large concentrations of dense lava in the flat seas on the lunar surface (called *mascons*). They make the gravitational field of Moon very irregular, resulting in unstable lunar orbits. Spacecraft in low-altitude orbits without any periodic control from onboard propulsion systems eventually crash into the Moon's surface [6, 7]. Therefore, it is critical to evaluate various lunar orbits and select the most feasible orbits for lunar mapping satellites that are nearly circular, polar and require minimal control thrust for long mission lifetimes. Further, low-thrust propulsion hardware and control strategies for application in such missions must be studied and optimized.

Although reliable technology is available to place spacecraft around the Moon in desired orbits, maintenance of such orbits over long periods is challenging because of perturbations from the gravity field of the Moon, Earth, Sun, and phenomena such as solar radiation pressure. Also, to obtain a near Sun-synchronous orbit, the ascending node

of the orbit must change at a Sun-synchronous rate which further increases the need of control with onboard propulsion systems. The stationkeeping requirements for lunar mapping satellites are strict; the low altitude provides only a narrow margin for error, creating a need for continuous orbit corrections. Lunar missions can exploit recent advancements in electric propulsion, which have been proven to provide continuous thrust at high specific impulses, available at different power levels. Studies and application of electric propulsion systems have shown increased payload size and on-orbit operational lifetime, making them the perfect solution to obtain the continuous control required to maintain various lunar orbits. The use of continuous electric propulsion can be used to obtain a wide variety of performance enhancing options for lunar mapping and communication, which have not been considered due to the traditional impulsive control strategy.

1.2. THESIS OVERVIEW

The research presented in this thesis is intended to aid in the selection of orbits for lunar mapping and communications satellites. It studies the impact of using electric propulsion (to control lunar orbits) on the search space of feasible and useful lunar orbits. This is done by evaluating the use of Sun-synchronous orbits for lunar mapping and geo-synchronous orbits for lunar communication. Propulsion requirements for continuous position control of satellites in such lunar orbits are investigated, to determine if electric propulsion is a feasible option for control. The control thrust is computed using a robust suboptimal control approach that calculates minimal control forces required to maintain the spacecraft in the desired trajectory.

The challenge of this research was to first develop a dynamic model of the system incorporating perturbations from the nonspherical Moon as well as from the Earth, the Sun, and solar radiation pressure. Secondly, a nonlinear control strategy that would be appropriate for a range of state and control weights had to be formulated and implemented to maintain spacecraft in desired orbits. Finally, a comparison of a wide selection of useful and possible lunar orbits had to be made, to recommend orbits for various lunar missions, which would benefit from electric propulsion and provide better performance. The remaining sections of this thesis are organized as follows:

Section 2 provides a review of research studies and investigations focusing on lunar orbits, control techniques, and electric propulsion hardware and applications. It also provides a brief insight on the considerations of possible research contributions adopted to be explored in this thesis.

Section 3 presents the derivation of the equations of motion used to determine the spacecraft's trajectory. The dynamics of problem is modeled using these derived nonlinear equations of motion that take into account the nonspherical shape of Moon and incorporates perturbations from other bodies involved (the Earth and Sun are considered as point masses).

Section 4 proposes a robust suboptimal controller that computes accurate control accelerations to maintain a spacecraft in desired orbits for various mission scenarios. This control method utilizes the state dependent algebraic Riccati equation (SDRE) approach to solve for the needed control.

In Section 5, numerical results which include histories of control acceleration, and errors in orbital elements, plotted with respect to time are presented to demonstrate the effectiveness of the control method and to find if electric propulsion is a practical alternative for lunar orbit control.

Finally, Section 6 concludes the thesis with a discussion on the contributions and findings of this research, and proposes future work in this field.

2. LITERATURE REVIEW

2.1. LUNAR ORBITS

Requirements for future lunar communication and navigation as detailed in [26, 29] recommend that early communications satellites (2010-2019) support robotic and human activities at the Moon's south pole to aid in building a lunar base and that the final communications satellite systems (2019 and after) provide global coverage of the entire lunar surface to support human exploration. The irregular and nonspherical gravity field of the Moon makes it impossible for most satellites to have long operational lifetime. Future lunar mapping missions will require satellites to operate at low altitudes in circular polar orbits (and if possible with a Sun-synchronous orientation). To meet these requirements the spacecraft must perform continuous maneuvers. However, due to limitations in fuel available for such maneuvers it is critical to select lunar orbits which provide a good tradeoff between acceptable position errors and control thrust required.

Communication with and tracking of spacecraft were among the major issues present during the Apollo missions. To address such problems and provide guidance for future lunar missions, Neuner [15] compared two possible lunar satellite systems which could be used for communication. The first being a system of uncontrolled satellites in random polar orbits, and the second being a system of two to six geo-synchronous lunar satellites in precise controlled orbits. He concluded that, although the development of a system of synchronous satellites would require high capital, in the long run it would be considerably less expensive than a communication system with uncontrolled satellites in polar orbits. In 1970, Farquhar proposed placing a satellite in a halo orbit at the Earth-Moon L_2 libration point to provide communications to the far side of the Moon [16, 19]. Motivated by this proposal, Carpenter and his colleagues [17] described how a constellation of four satellites in Earth-Moon L_2 halo orbits could provide continuous coverage of the lunar far side and the poles. Later in 2006, Grebow together with Howell, Ozimek, and Folta proposed using just two satellites in halo orbits to provide constant coverage of the lunar south pole region, which is the region chosen for a lunar base [18]. Despite the great interest in halo orbits, multiple launches are required to place spacecraft in the proper L_2 orbits. Each launch adds expense and could lead to delays for other lunar

missions dependent on the constellation. Also, the use of these unstable halo orbits requires frequent stationkeeping maneuvers [19]. To avoid this, constellations of elliptical inclined frozen lunar orbits that have no secular change in orbital elements due to perturbations, have been proposed for polar and global coverage of the Moon by Ely and Lieb in [20]. They proposed a constellation of three satellites for persistent and stable polar coverage of the Moon and then extended this idea to a constellation of six satellites that provide 100% global lunar coverage for ten years. For polar coverage, three satellites could be placed in the same orbit plane, defined by the following characteristics: semimajor axis, a = 6541.4 km; eccentricity, e = 0.6; inclination, i = 56.2 deg; longitude of ascending node, $\Omega = 0$ deg and argument of periapsis, $\omega = 90$ deg. For global coverage, six satellites could be placed in two orbits (three in each) defined as: semimajor axis, a = 7500 km; eccentricity, e = 0.05; inclination, i = 40 deg; longitude of ascending node, $\Omega = 0$ and 90 deg; and argument of periapsis, $\omega = 90$ and 270 deg.

Park and Junkins [21] were among the first to study the behavior of different lunar mapping orbits under the influence of lunar gravity. They used the concept of frozen orbits to establish a family of near circular polar frozen lunar mapping orbits that provide global coverage in one month. After describing why it is not feasible to obtain a Sun-synchronous polar orbit without control force, they provide a set of relatively stable lunar mapping orbits that ensure that the Sun would always be within 10.2451 deg of the Sun-synchronous constraint. One such orbit is described as having the following classical elements: semimajor axis, a = 1837.63 km; eccentricity, e = 0.0013089; inclination, i = 101.5deg; longitude of ascending node, $\Omega = 189$ deg; and argument of periapsis, $\omega = 90$ deg.

Ramanan and Adimurthy [23] later analyzed the influence of lunar gravity field harmonics on different near circular polar lunar orbits to find low lunar orbits that have long operational lifetime with minimal or no control thrust application. They studied the impact of changing inclinations and ascending nodes on the lifetime (which is directly related to the stability in periapsis altitude) of near circular low altitude lunar orbits. Their results show that most stability in the periapsis altitude of a mapping satellite is obtained at close to 95 deg inclination and near 0 deg ascending node.

Perturbations on Earth orbiters are mainly due to J_2 through J_5 gravity terms, but lunar orbits have nonuniform perturbations due to irregular distribution of lunar mascons and perturbations from Earth [24]. Quinn and Folta argued that frozen orbits provided by Park, Junkins [21], Ely [20], and Lara [22] are limited to zonal potential terms of degree nine. They further study lunar frozen orbits and present an analytical formulation followed by numerical simulation to select usable lunar orbits that reduce or eliminate the need of stationkeeping. They proposed a frozen orbit condition of: semimajor axis, a = 1861 km; eccentricity, e = 0.043; inclination, i = 90 deg, for North Pole coverage, and a 12 hour high inclination, high eccentricity orbits (i = 62 deg, e = 0.6 or i = 45 deg, e = 0.4) for South Pole coverage. Their solution for global coverage is a system of eight to twelve satellites in frozen lunar orbits characterized by a semimajor axis, a = 8049 km; eccentricity, e = 0.4082; inclination, i = 45deg.

Russell and Lara [25] noticed that frozen orbits are generally found by seeking equilibrium solutions to an averaged or reduced system that discards the effects of many higher-order perturbations. To solve for repeat ground track lunar orbits that represent higher order solutions to lunar frozen orbit problem, they use a differential correction technique after superimposing a high resolution lunar gravitational field on the Earth-Moon Restricted Three Body dynamic model, capturing the dominating forces on a spacecraft in the vicinity of the Moon. They showed that for near-polar orbits minimum variations in eccentricity occur near i = 85 deg and i = 95 deg and minimum variations in altitude occur at i = 94.8 deg. Some of the promising frozen orbits presented by them include

1) an inclined circular high altitude lunar frozen orbit with a = 5046.74 km, e = 0.000242, i = 70.64 deg, $\omega = -40.49$ deg and $\Omega = 177.63$ deg,

2) an inclined eccentric high altitude lunar frozen orbit with a = 4996.65 km, e = 0.5384, i = 52.21 deg, $\omega = 89.22$ deg and $\Omega = 146.72$ deg, and

3) a low-altitude near-circular near-polar lunar frozen orbit with a = 1861.79 km, e = 0.0211, i = 92.98 deg, $\omega = -7.84$ deg and $\Omega = 158.95$ deg.

The Space Communication Architecture Working Group (SCAWG) at NASA has designed a Space Communication Architecture [26] that will provide the necessary communication and navigation services for space exploration and science missions

planned for the next twenty years. This architecture presents a trade study of many lunar coverage constellations and recommends the most suitable candidate for zonal and global lunar communication. The selection is done by a Figure of Merit (FOM) definition based on visibility, changeability, failure tolerance, complexity, evolvability, stability etc. The FOM scores are studied against life-cycle cost to measure and assess each alternative. Almost all feasible options for lunar coverage are included in the study. These lunar relay options include constellations of inclined elliptical orbits, inclined circular orbits, halo orbits, hybrid orbits and Malapert stations. The results of the study show that two satellites in an elliptical inclined high-altitude frozen lunar orbit with a 12 hr time period (a = 6142.4 km, e = 0.5999, i = 57.7 deg, and $\omega = 90$ deg) [28] provide the highest FOM score at low cost and is recommended as the best choice for polar coverage. This is followed by a constellation of three satellites in inclined high altitude circular orbits (a = 6430 km, i = 70 deg). Also, for global coverage, the recommended architecture is a constellation of six satellites, divided in two high altitude frozen orbits with three satellites in each placed by two launches.

2.2. DEVELOPMENTS IN ELECTRIC PROPULSION SYSTEMS

Electric propulsion systems in general are characterized as continuous low-thrust, high specific impulse propulsion systems. They are known to improve a wide variety of orbit maneuvering and maintenance missions in terms of deliverable payloads and on-orbit lifetime [30]. Electric propulsion systems cannot produce sufficient thrust to lift payload through the Earth's atmosphere, but they are an efficient propulsion source in frictionless space. Recently, the use of electric propulsion systems is being considered as a viable alternative to the classical chemical actuators, and is rapidly becoming the baseline for new telecom satellite platforms [31, 52]. Electric propulsion has been utilized in numerous communications satellites and a few deep space missions, including Deep Space 1 (NASA), Hayabusa (Japan), and Dawn (NASA). Currently, 180 spacecraft in operation use electric propulsion systems [32]. In 2004, the spacecraft SMART-1 (Europe) demonstrated the use of electric propulsion by raising its orbit from a geostationary transfer orbit to the Moon. The spacecraft (367 kg) was equipped with an 82-kg xenon fuel tank and a PPS-1350G xenon Hall thruster [40] designed by Snecma

and having a mass of 27 kg. The thruster operated at power levels ranging from 462 to 1190 W provided by the solar arrays.

Groot [33] classifies electric propulsion devices in three classes: electrothermal, electrostatic and electromagnetic devices, based on the principle by which the working fluid is accelerated to provide thrust. In electrothermal thrusters, a high temperature fluid is accelerated through a conventional nozzle to provide a driving force. Electromagnetic thrusters provide thrust by accelerating a charged plasma by means of an electromagnetic field. Electrostatic thrusters on the other hand use a static electric field to accelerate an electrically charged plasma.

Electrothermal propulsion systems include resistojets that use a coil to heat the propellant, usually hydrazine, and arcjets that use a stationary arc to excite the propellant. Aerojet, a company that specializes in missile and space propulsion, has designed a 500 W resistojet named the Aerojet MR-501B Electrothermal Hydrazine Thruster (EHT) that generates up to 360 mN of thrust and specific impulses (Isp) of 303 sec. This resistojet is commonly used for communications satellite stationkeeping, and over 200 Aerojet EHTs have already flown since 1983 [45, 46]. NASA's Lewis Research Center and Olin Aerospace Corporation are jointly working on several varieties of arcjets for use in stationkeeping of satellites. Exhaust velocities of 1000 to 5000 m/s have been demonstrated with thrust ranges of 0.01 N to 0.5 N and specific impulse of 520 sec at 1.8 kW power input. This 1.8-kW hydrazine arcjet has been approved for use on Lockheed Martin Series 7000 geosynchronous telecommunications satellites to provide a highly efficient means of north/south stationkeeping [47]. However, electrothermal propulsion continues to present issues and concerns related to the control of propellant flow rate and heat transfer, especially for small and compact satellite applications.

Pulsed plasma thrusters (PPT) are electromagnetic thrusters known for their light weight and very low thrust levels, which makes them ideal for attitude control, precision spacecraft control, and low-thrust maneuvers of small spacecraft [43, 50]. PPTs have a solid propellant bar, usually Teflon, spring loaded inside an insulating container. A capacitor discharge strikes an arc on the propellant surface that vaporizes molecular layers of propellant, creating a plasma [33]. The same discharge also generates an electromagnetic field that accelerates the plasma to provide a small thrust pulse typically

between 0.05 and 2 mN at an Isp of around 2000 sec. NASA's Earth Observing 1 (EO-1) spacecraft launched in 2000, used one dual-axis PPT for pitch axis control and momentum management [38]. The Variable Specific Impulse Magnetoplasma Rocket (VASIMR) is another electromagnetic thruster for spacecraft propulsion. It uses radio waves to ionize a propellant and magnetic fields to accelerate the resulting plasma to generate thrust [51]. The VX-200 which is a VASIMR, is currently being developed by Ad Astra Rocket Company and is scheduled to be installed on the International Space Station in 2011-12 for testing. It is expected to show produce thrust levels up to 5 N at an efficiency of 60% and Isp of 5000 sec using a low-cost argon propellant.

Electrostatic thrusters that include ion and Hall effect thrusters have recently become the most popular choice for control of spacecraft. New developments and tests have shown that such thrusters are very efficient even at high power levels and produce high thrusts compared to other electric thrusters. They also have long operating lifetime and provide significant payload mass savings. In an ion thruster, a plasma is created from a propellant (usually xenon) by means of an electrical discharge in the discharge chamber. The plasma is accelerated in an electrostatic field created by a set of ion grids placed at the exit of the thruster [33]. Edward and Gabriel in [35] describe four ion thrusters with thrust capabilities between 20 to 200 mN and high specific impulses (typically 2000-5000 sec), with power requirements ranging from 2.5 to 7 kW depending on the required thrust level.

The Dawn spacecraft [36] was launched by NASA in 2007 on a mission to explore the two largest members of the asteroids belt, Vesta and Ceres. It was equipped with three xenon ion electric propulsion engines (powered by solar arrays) that have a specific impulse of 3100 sec and can produce thrust up to 90 mN. The capabilities of Dawn's propulsion system have been evaluated at five throttle levels, and the engine has performed flawlessly. Results also show that after 27 hours of thrusting from the ion engine, less than 0.28 kg of the spacecraft's xenon fuel supply was consumed. Dawn's fuel tank carries 425 kg of xenon propellant, which will provide enough propellant to Dawn's ion engines for about 50,000 hours (over five years) of operation [36]. The Dawn spacecraft is scheduled to rendezvous with Vesta in 2012, and its ion propulsion will provide the additional velocity needed to reach Vesta after leaving the Delta rocket. In

2015, Dawn will also use its ion propulsion system to spiral around Vesta and Ceres in low altitude orbits.

NASA's Evolutionary Xenon Thruster (NEXT) [34] is the next generation ion propulsion system currently being developed by NASA's Glenn Research Center, Jet Propulsion Lab and Aerojet. This thruster operates at an input power level ranging from 0.54 to 6.9 kW. At full power, the thruster has a peak efficiency of 70%, a maximum thrust higher than 236 mN and an Isp greater than 4170 sec. Engineering models of these xenon ion propulsion systems have been tested successfully at their maximum power levels for 2000 hours. Also, a string system that fires three ion thrusters simultaneously has been tested at 20.6 kW total input power, yielding a total thrust of about 710 mN at an Isp of 4190 sec and an efficiency of approximately 71% [34].

Another electrostatic thruster is the Hall effect thruster. Busek Co., which specializes in electric propulsion, has been developing the next generation high-performance Hall effect thrusters for the last 12 years. They have designed a family of BHT Hall effect thrusters that span the power spectrum from 200 W to 20 kW and produce 5 mN to 1 N of thrust with specific impulse values varying between 1000 and 3000 seconds. BHT-20K, the largest Hall thruster designed by Busek, was tested at the NASA Glenn Research Center in 2005 and can produce 1.09 N of thrust at 2750 seconds specific impulse and 70% efficiency. TechSat-21, a constellation of three satellites used by the Air Force Research Lab (AFRL) to demonstrate satellite formation operations, is equipped with BHT thrusters as the primary propulsion system [48, 49].

As part of project Prometheus, NASA's Glenn Research Center has developed the 457-M Hall Thruster. This thruster is 50-kW high power Hall thruster and uses krypton as the propellant instead of xenon [41]. This thruster has been tested over a range of 8.5 to 74.0 kW to produce thrust levels ranging from 390 mN to 2.5 N at a discharge Isp of 4500 sec and peak efficiency of 64%. Advancements in electric propulsion systems by Aerojet is been discussed by Wilson in [37]. Aerojet is currently producing a 4.5-kW Hall Thruster Propulsion System (HTPS) that can provide propellant mass savings up to 900 kg for large GEO communications satellite missions. These Hall thrusters can provide thrust levels ranging from 161 to 282 mN at power levels between 3 to 4.5 kW.

Figure 2.1 Thrust and Isp for Different Propulsion Systems [Ref. 36]

Ground testing of NASA's High Propulsion Electric Ion thruster (HiPEP) [44] has demonstrated a very efficient (80%) thrust production of 670 mN and an Isp of 9620 sec at a power input of 39.3 kW. HiPEP uses a combination of microwave and magnetic field to produce thrust; it was intended to be used in NASA's JIMO (Jupiter Icy Moons Orbiter) Mission cancelled in 2005.

To achieve the objectives of a station keeping, most satellites equipped with chemical propulsion systems use an impulse control strategy to compensate for changes in the orbit parameters. Although a chemical propulsion system on a spacecraft might have a thrust of up to 500 N (see Figure 2.1), electric propulsion engines can achieve an equivalent trajectory change by firing the thrusters over a much longer period of time. Before using electric thrusters, it is therefore necessary to re-think the control strategy as a continuous process and optimize its application [31]. The current state-of-the-art electric propulsion systems are based on hydrazine electrothermal systems but with

recent advancements in electrostatic ion and Hall thrusters a wide variety of options are available.

2.3. CONTINUOUS LOW-THRUST ORBIT CONTROL

In the past much interest has been seen in continuous low-thrust stationkeeping and maneuvering of spacecraft, especially with recent developments in electric propulsion systems. Oleson, Myers and Kluever [59] in 1997, for example, analyzed the use of solar electric propulsion for stationkeeping and insertion of a spacecraft into a geostationary orbit. They showed that a significant increase in payload mass can be obtained by performing portions of the orbit transfer using advanced solar electric propulsion systems. Later in 2000, Oleson [65] studied the effect of changes in electrostatic thruster performance by variation in specific impulse on trip time and allowable payload mass for different phases of such space missions. He showed that application of variable specific impulse devices offer 5 to 15 % increase in payload mass.

What follows is a review of a few of the numerous other research studies that, motivated by the many advantages that electric propulsion has to offer, investigate and optimize the use of continuous low-thrust propulsion systems for a variety of interesting space missions.

Hunziker was among the first to investigate low-thrust control of orbits. In his work (published in 1970, [52]), he discussed low-thrust stationkeeping of a spacecraft in a circular equatorial orbit. He used the method of variation of parameters to minimize the change in spacecraft longitude in an effort to maintain it directly overhead a certain point on the Earth.

Losa et al. [62] considered the modeling and control issues associated with using electric propulsion for station keeping for geostationary satellites. They used a direct method, differential inclusion, to solve this continuous optimal control problem. This method incorporates explicitly defining control as a function of the state and its derivatives such that the control bounds can be translated to allowable bounds in the state. Palutan et al. [58] explored a model based on genetic algorithms for stationkeeping of geostationary satellites by ion thrusters. This algorithm allows convergence to an optimum solution for stationkeeping after successive iterations and inputs from the user.

Gurfil [64] examined the problem of continuous thrust orbital transfer utilizing concepts of controllability and feedback stabilizability. He used Gauss's variational equations to model the state-space dynamics of spacecraft motion under a central gravitational field and derived a controller to steer a spacecraft from an initial elliptical orbit to any given elliptical orbit. His results demonstrate that a low-thrust continuous controller requires less fuel than an impulsive maneuver for the same transfer time.

Kluever has published several papers that analyze orbit transfers using solar electric propulsion. For example, in [57], he used a direct optimization approach to solve an optimal control problem that computes minimum–time low-thrust Earth orbit transfers. Such transfers include transfer from low Earth orbit (LEO) to geosynchronous orbit (GEO) and geosynchronous transfer orbit (GTO) to GEO. In [60], he investigates the feasibility of using electric propulsion for a comet rendezvous mission. He uses an Earth gravity assist to increase the orbital energy and conserve propellant for a rendezvous trajectory to the comet Wilson-Harrington. He also incorporates a detailed treatment of the spacecraft system mass breakdown and lifetimes of ion thrusters in the trajectory optimization process.

Sidi [56] investigated control and guidance laws for low-thrust coplanar orbit transfer maneuvers. He proposed a guidance law based on classical control theory, which is fairly insensitive to uncertainties in control parameters including thrust level, thrust direction, and initial maneuver time. This law minimizes a performance index based on a trade-off between time and fuel expenditure making it useful for missions in which the maneuver must be performed in a single phase because of operational time constraints.

Edelbaum [61] determined analytic solutions for optimum corrections of all six elements of elliptic satellite orbits with power-limited propulsion systems. The optimum direction and magnitude of thrust were determined as functions of time to minimize the fuel required to rendezvous in a given time or to minimize the fuel required for stationkeeping in the presence of known perturbations. Gomes et al. [63] used a suboptimal parameterization control method to compute the minimum thrust required to maneuver a satellite to its position in a constellation of satellites from a parking orbit.

Electric propulsion maneuver strategies have also been proposed for avoiding collisions in space. Peissinger [54] developed a model based on optimal control theory to

find continuous thrust vectors aimed to maximize the distance between a threat and the target satellite. He presented minimum-time solutions for maneuvering a satellite under attack out of a volume space in which its destruction is highly likely. Widhalm and Eide [55] used optimal control theory to derive two-point boundary value problems that are solved numerically to obtain the continuous low-thrust required to perform in-plane maneuvers to avoid collisions and threats from other satellites. They also studied the time and thrust required to reposition a satellite into its nominal orbit after performing a safety maneuver.

Harl and Pernicka [76] are among the first to investigate control of future lunar mapping orbits. They used optimal control theory to design a controller for low-thrust control of a spacecraft in Sun-synchronous lunar mapping orbit. They developed a cost function aimed to control the inclination and ascending node of a spacecraft in a Sun-synchronous lunar orbit. Simulation results presented in [76] show that a maximum control thrust of 0.76 N, is required to maintain a tolerance less than 0.3 deg in the inclination and ascending node tracking, for a 1000 kg spacecraft. However, their approach did not account for changes in semimajor axis and eccentricity, because of which the spacecraft looses 40 km in altitude in just 50 days. Recently, at a research conference, they presented an update [94] on their study, in which they modify the cost function to allow them to control all orbital elements and the periapsis altitude. They use finite differences and shooting method to solve the optimal control problem. Their newer results show that continuous control forces below 1 N are sufficient to control Sun-synchronous orbits for any amount of time.

2.4. NONLINEAR CONTROL METHODS

The ideal or desired motion of a spacecraft is perturbed by many uncertain and nonlinear forces, including gravitational forces, drag, solar radiation pressure, etc. Orbit maneuvering is a term associated with the use of propulsion systems to change or maintain the orbit of a spacecraft to a desired one. The efficiency of an orbital maneuver is usually measured by the amount of fuel (proportional to thrust required) and time required to perform the maneuver. For continuous low-thrust, the goal is to minimize the difference between the current state of the spacecraft and the desired state of the

spacecraft and minimize the control thrust required to do so. Such problems are commonly known as tracking problems.

Many nonlinear control techniques have been proposed and used to solve tracking problems; each of them performs differently for different systems, and each has its own advantages and drawbacks. Zhang and Li [66], for example, developed an adaptive control strategy based on feedback linearization to control a chaser satellite flying around a target satellite while maintaining a desired relative position and attitude. Feedback linearization is conceptually the simplest form of nonlinear control; it is achieved by cancelling or transforming the nonlinear dynamics of the system into a linear-like structure. Once the nonlinearities in a system have been cancelled, linear control techniques can be implemented to obtain the required control inputs, but this method can only be applied if the zero dynamics of the system is stable. Even if a system is feedback linearizable, the control inputs obtained may not be feasible because the input needed to cancel the (sometimes beneficial) nonlinearities may be exceedingly large [67].

Terui [68] demonstrated the use of a sliding mode controller for position and attitude control of a spacecraft. The sliding mode control methodology is based on a notational simplification, which amounts to replacing an *n*th order tracking problem with a first order stabilization problem [67]. This method is also called variable structure system control, and it is based on a high frequency switching control law that changes depending on the state trajectory. Sliding mode controllers are known for their fast response and good robustness, but due to high control gains they often result in a chattering control input that can damage the equipment [70].

Nonlinear backstepping is another control method that is based on the Lyapunov theory and has been effectively applied to many problems. The drawback of conventional backstepping is that it can only be applied to systems that are feedback linearizable; thus, backstepping is used in conjunction with various other techniques like adaptive control, optimal control, neural networks etc. Kim [69] proposed a modified backstepping method based on Lyapunov redesign to control rigid spacecraft slew maneuvers. The complexity of this control method, however, has always been an issue.

Optimal control theory, on the other hand, has been successfully applied to a wide variety of problems and is well documented in many texts and research articles [72, 73,

54-58, 62]. This theory provides a set of differential equations which can be integrated to determine state and control trajectories that minimize a performance index, i.e., a cost function. In general, these equations are solved using direct or indirect optimization methods. Indirect methods include shooting methods and backward sweep algorithms. They solve an optimal control problem by obtaining the solution to a two point boundary value problem (TPBVP), obtained after using the calculus of variations. A drawback of indirect methods is that the TPBVP is usually very sensitive and extremely difficult to solve unless a good initial guess is available. However, if the solution to the TPBVP is obtained, the resulting trajectory in most cases is optimal. Direct methods solve an optimal control problem by adjusting the control variables at every iteration in an attempt to continually reduce the performance index [75]. This makes direct methods like collocation and direct transcription very robust but slowly convergent to the solution [76].

Two special cases of an optimal control problem are the regulator problem and the tracking problem; the performance index for both is a quadratic function of the state and control. The basic difference between the two problems is the objective. For a regulator problem, the objective is to maintain a steady state; for a tracking problem it is to follow a predetermined trajectory [72]. Thus, in a regulator problem the desired state is constant or zero, and in a tracking problem the desired state is changing. The quadratic performance index chosen for these problems provides an opportunity for the control law to be a compromise between state error and control input, thus making the method more robust. Solutions to tracking optimal control problems require computation of feed forward terms [73, 80] that involve backward integration from the final condition. To achieve an optimal solution for infinite horizon nonlinear tracking problem, such computations are almost impossible. Direct solutions to tracking problems are investigated by Barbieri and Alba-Flores in [81, 82], but these solutions are only applicable for linear systems. A tracking problem, however, can be viewed as an independent regulator problem in each time step.

In 1990s, Cloutier et al. [83, 84] popularized the state dependent Riccati equation (SDRE) based suboptimal approach for solving regulator problems. Since then, this approach has been applied to a variety of control problems with good results. This

method is numerically very simple and requires no tedious work, like multiple differentiations of highly nonlinear dynamics, to derive necessary optimality condition. The SDRE feedback approach for regulator problems has been shown to be optimal for the scalar case as well as locally asymptotically stable and locally asymptotically optimal for multivariable cases [74].

Stansbery and Cloutier [77] were the first to show how the position and attitude of a spacecraft can be controlled using the SDRE Technique (SDRE). Later, Luo and Chu [78] demonstrated how the state and control weight matrices can be scheduled to constrain the control required and improve SDRE results. Ming, Balakrishnan and Stansbery in [79] utilized a new suboptimal control technique called the θ-D technique to obtain closed-form solutions for position and attitude control. This method overcomes SDRE controller's implementation problem, which occurs due to the fact that SDRE controllers require online computation of the Riccati equation at every time interval. However, all these papers use a very simple and unrealistic model of the spacecraft's dynamics that assumes a rigid spacecraft and neglects gravitational forces to demonstrate the suboptimal controller.

2.5. THESIS CONSIDERATIONS AND PROPOSALS

The current state of electric propulsion hardware (as surveyed in Section 2.2), provides a variety of electric propulsion options available for thrust levels up to 1 N. Furthermore, NASA's 457-M Hall thruster, that uses krypton as the propellant, can produce thrust levels up to 2.5 N. Electric propulsion engines can be used in a string system that fires more than one thruster simultaneously to obtain higher thrust values, if required. A spacecraft can also use multiple low-thrust engines oriented in different directions, to obtain an overall higher range of continuous but varying control thrust vectors.

Comparison and examination of the different control methods show that the SDRE technique overcomes many of the difficulties and shortcomings of existing control methodologies, and delivers a computationally simple algorithm that can be applied to a wide variety of control problems. This technique can be viewed as an extended feedback linearization technique, which preserves the beneficial nonlinearities of a system, and

additionally offers great design flexibility and robustness through state-dependent weighting matrices, with the capability of imposing hard bounds on the control and its behavior [67, 74]. The SDRE feedback control law satisfies the necessary conditions for optimality, but it does not necessarily provide a control trajectory that minimizes the performance index globally. However, optimality is not the primary concern for this study, given the flexibility and simplicity offered by the suboptimal SDRE technique. Striving for a control algorithm that is systematic, simple, and yet optimizes the performance, providing tradeoffs between control effort and state errors [74]; the SDRE technique is chosen and used in this research to design a continuous controller that works for various lunar orbits.

Traditionally, lunar orbit control has been done using an impulsive control strategy, in which the thrusters are fired once every few weeks to restrict any drifts of the spacecraft from its desired trajectory. Preferable lunar mapping orbits are circular, polar and low altitude Sun-synchronous orbits. These orbits are highly unstable and have very short lifetimes due to the irregular and nonspherical gravity field of Moon. Furthermore, unlike Earth, the Moon's gravitational field does not possess sufficient oblateness to provide the Sun-synchronous rotation of ascending node. Impulsive control is an undesirable option for controlling low-altitude lunar orbits, as they tend to require large control forces that can only be provided by engines which impose high payload mass requirements (for carrying fuel) on mission design and offer a limited operational lifetime. Unless, impulse thrusters are fired more rapidly it is difficult to maintain the state errors of the spacecraft within an allowable margin for low-altitude highly accurate lunar mapping. Continuous low thrust by solar powered electric propulsion is a good choice to obtain the highly desired mapping conditions provided by low altitude, circular, polar orbits.

Frozen orbits are characterized by no long-term changes in orbital eccentricity, inclination and argument of periapsis. Proposed architectures for lunar communication recommend frozen lunar orbits with high altitude to provide high nadir angles which makes more lunar surface available under the coverage area. Those for south pole coverage recommend frozen orbits with high semimajor axis; argument of periapsis, $\omega = 90$ deg and high eccentricity to make the spacecraft spend the most time over the

south pole at high altitudes for maximum coverage. Recent trade studies [26, 27, 28] by NASA, show that the most feasible and least expensive option for lunar south pole coverage is a system of two satellites in a highly elliptical and inclined frozen orbit, with its apoapsis over the south pole (a = 6142.4 km, e = 0.5999, i = 57.7 deg, and $\omega = 90$ deg). This architecture is not only highly stable (because of its frozen orbit) but is also easily evolvable into a near-global coverage system by simply placing two more satellites in the same orbit but with a northern apoapsis ($\omega = 270$ deg). However, this architecture requires two rocket launches and the performance of the constellation changes significantly as the apoapsis rotates in longitude due to the motion of the Moon about Earth. Thus, when the apoapsis is over the near-side, the far-side coverage drops, and when the apoapsis is over the far-side, the coverage peaks (considering direct communication with Earth for the near-side) [95]. The long-term effects of all the perturbations make a frozen orbit essentially non-frozen, affecting the operational lifetime of the constellation, because of which frozen orbits also need occasional impulse maneuvers.

Although, continuous propulsion is not a good option for frozen orbit control, better and more effective lunar coverage is possible using high altitude geo-synchronous orbits for which continuous control is an efficient option. Just like Sun-synchronous orbits which are fixed with respect to Sun, geo-synchronous orbits are fixed with respect to Earth. For geo-synchronous the required the rate of change in the ascending node, $\dot{\Omega}$ is equal to the rate at which the Moon revolves around Earth i.e. $\dot{\Omega} = 360\,\text{deg per } 27.32\,\text{days}$. If the continuous control required to provide this geo-synchronous orbit plane rotation at high altitude is modest, then more feasible and performance-enhancing alternatives become available for lunar communication rather than just constellations of frozen orbits. One such alternative is being proposed in this thesis. It is a constellation of three satellites in high-altitude, circular and polar geo-synchronous orbit with the orbit plane always facing the Earth. This architecture requires only three satellites, which can be placed in orbit with a single rocket launch instead of the four satellites and dual rocket launches required while using inclined frozen orbits. The proposed constellation provides continuous near-global lunar coverage with full coverage at the poles and only a small equatorial region on the far side not directly visible, as seen in Figure 2.2. Nevertheless, it

provides more than one relay available for low altitude satellites flying over the uncovered region. Also, the constellation is not affected by the Moon's motion as the orbit is geo-synchronous and remains fixed as seen from Earth.

Figure 2.2 Lunar Coverage with Three Geo-Synchronous Satellites

With an aim to aid in proper selection of future lunar mission orbits, the research presented in this thesis shows the impact of using electric propulsion (to control lunar orbits) on the search space of feasible and useful lunar orbits. It

a) evaluates the use of Sun-synchronous orbits for lunar mapping and geo-synchronous orbits for lunar communication;
b) justifies and demonstrates the use of SDRE for nonlinear spacecraft position control using a high fidelity dynamic model;
c) examines if continuous thrust is a viable option for controlling the behavior of lunar orbits, and to satisfy various mission requirements;
d) determines if the current technology is capable of providing continuous thrust required to control lunar orbits;
e) explores the possibility of an analytic control law for various lunar orbits to minimize the online computation required for control calculations.

3. DYNAMICS OF THE SPACECRAFT

The equations of motion for a spacecraft orbiting the Moon perturbed by the gravitational potential of the nonspherical Moon, the Earth, and the Sun as well as accelerations caused due to solar radiation pressure are derived and discussed in this section. These equations of motion are a mathematical representation of the system in consideration and are used to find the accurate position and velocity of the spacecraft at any time.

3.1. COORDINATE FRAMES AND TRANSFORMATIONS

The equations of motion are derived relative to a selenocentric reference frame. The inertial frame is fixed at a point '*I*' in inertial space and is denoted by $(\hat{X}, \hat{Y}, \hat{Z})$. A relative coordinate system, i.e., a rotating frame is used, to make the expression and propagation of spacecraft's position and velocity vectors easier. The mean selenographic frame [86] is used as the rotating reference frame and is denoted by $(\hat{\mathbf{x}}, \hat{\mathbf{y}}, \hat{\mathbf{z}})$. The $\hat{\mathbf{x}}$ unit vector lies in the equatorial plane of Moon and is directed from the center of Moon towards the center of Earth. The $\hat{\mathbf{y}}$ unit vector is defined normal to the $\hat{\mathbf{x}}$ unit vector and normal to the plane of the lunar prime meridian, and the $\hat{\mathbf{z}}$ unit vector is defined as the unit vector normal to $\hat{\mathbf{x}}$ and $\hat{\mathbf{y}}$ that completes the right-handed frame.

In order to conduct simulations, the inertial frame is considered to be the mean selenographic reference frame at the initial time. The inertial frame $(\hat{X}, \hat{Y}, \hat{Z})$ is centered at the Moon and has directions aligned with the directions of the rotating frame at the initial time. The rotating frame, i.e., the mean selenographic frame, however, is rotating as the Moon revolves around the Earth. Thus, the position of the spacecraft expressed in both the frames at the initial time is the same. However, the velocity and acceleration of the spacecraft with respect to both frames are, in general, different. Transformations between inertial and rotating frames are carried out multiple times during a simulation. This transformation is given by a single rotation (see Figure 3.1) of θ about the $\hat{\mathbf{z}}$ axis with $\theta = \omega_m . t$, $\dot{\theta} = \omega_m$ *and* $\ddot{\theta} = 0$ where $\omega_m = 2.661699$ x 10-6 rad/sec. ω_m is the angular rotation rate of the Moon which is nearly constant.

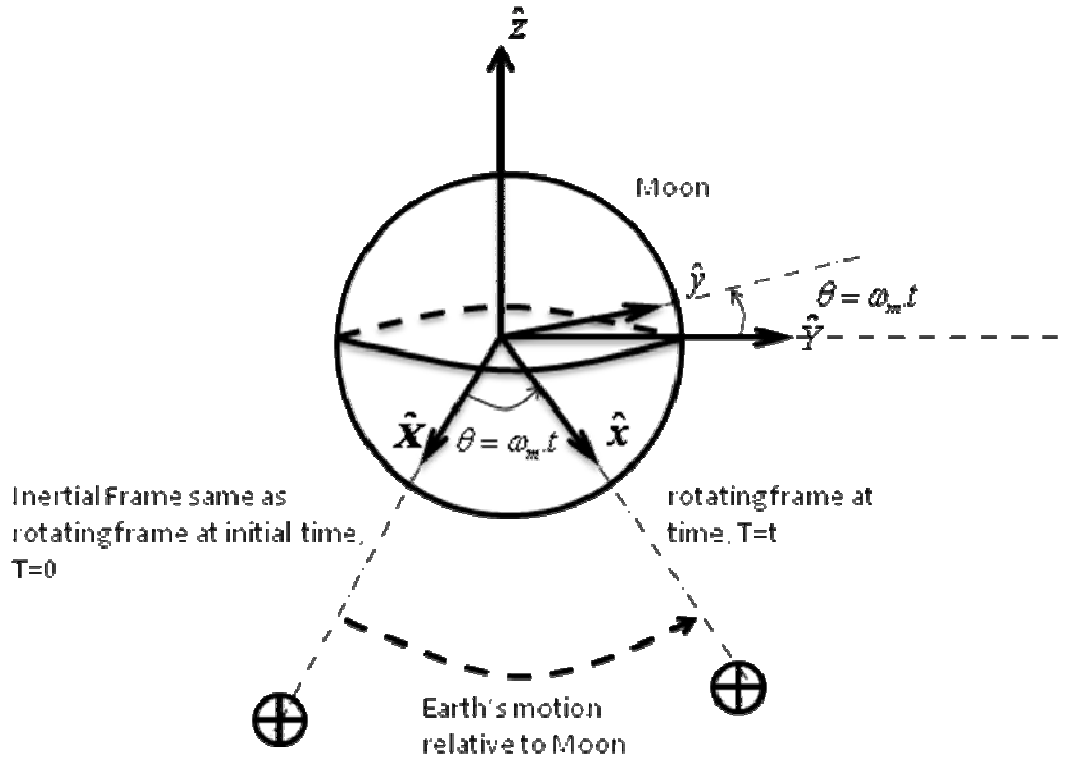

Figure 3.1 Transformation from Inertial Frame to Rotating Frame

The direction cosine matrix, DCM for the transformation is given by

$$DCM = \begin{bmatrix} \cos\theta & \sin\theta & 0 \\ -\sin\theta & \cos\theta & 0 \\ 0 & 0 & 1 \end{bmatrix}$$

$$\text{with } D\dot{C}M = \dot{\theta}\begin{bmatrix} -\sin\theta & \cos\theta & 0 \\ -\cos\theta & -\sin\theta & 0 \\ 0 & 0 & 0 \end{bmatrix},\ D\ddot{C}M = \ddot{\theta}\begin{bmatrix} -\cos\theta & -\sin\theta & 0 \\ \sin\theta & -\cos\theta & 0 \\ 0 & 0 & 0 \end{bmatrix}, \text{and} \tag{3-1}$$

$$\begin{aligned} \overline{r}_R &= [DCM]\overline{r}_I \\ \dot{\overline{r}}_R &= [DCM]\dot{\overline{r}}_I + [D\dot{C}M]\overline{r}_I = \dot{\overline{r}}_I - \omega_m \hat{z}\times\overline{r}_R \\ \ddot{\overline{r}}_R &= [DCM]\ddot{\overline{r}}_I + 2[D\dot{C}M]\dot{\overline{r}}_I + [D\ddot{C}M]\overline{r} = \ddot{\overline{r}}_I - 2\omega_m \hat{z}\times\dot{\overline{r}}_R - (\omega_m \hat{z}\times(\omega_m \hat{z}\times\overline{r}_R)) \end{aligned} \tag{3-2}$$

are used for the transformation, where the vectors $\overline{r}_R$, $\dot{\overline{r}}_R$, $\ddot{\overline{r}}_R$ and $\overline{r}_I$, $\dot{\overline{r}}_I$, $\ddot{\overline{r}}_I$ represent the position, velocity and acceleration of the spacecraft expressed in the rotating frame and the inertial frame respectively.

Transformations from the ecliptic frame to the rotating frame are also carried out as the positions of the Earth and Sun are expressed using the ecliptic frame. The ecliptic frame is defined using the plane of the Earth's mean orbit about the Sun as the fundamental plane. The origin of the ecliptic frame is at the center of the Earth and its $\hat{\mathbf{x}}$ axis always points toward the vernal equinox. The transformation of a position vector from the ecliptic frame ($\overline{r}_E$) to the mean selenographic rotating frame ($\overline{r}_R$) requires three rotations. The following steps are followed to find the three transformation angles and the direction cosine matrix (DCM) required for the conversion [86]:

Figure 3.2 Transformation from Ecliptic Frame to Rotating Frame

1. Find the centuries, T past Jan 0.5, 1990 given by
   $T = D/36525$ where $D = (JD - 2415020)$ i.e. Days past Jan 0.5, 1990 (3-3)
   such that JD is the current time expressed in Julian dates.

2. Find the geocentric mean longitude of the Moon, $\supset$ and the longitude of the mean ascending node of the lunar orbit, Ω using

$$\supset = 270.4341639^\circ + 481267.8831417^\circ T - 0.00113333^\circ T^2 + 0.1888889\times 10^{-5} T^3$$
$$\Omega = 259.1832750^\circ - 1934.1420083^\circ T + 0.002077778^\circ T^2 + 0.2222222\times 10^{-5} T^3 \quad (3\text{-}4)$$

3. Find the three Euler rotation angles, defined in Figure 3.2 as ϕ, θ, *and* ψ. These angles represent three rotations respectively about the *z* axis, the *x* axis resulting after the first rotation and the *z* axis resulting after the two rotations.

$$\phi = \Omega + \pi$$
$$\theta = I \quad (3\text{-}5)$$
$$\psi = \supset - \Omega$$

4. Find the DCM to make a coordinate transformation from ecliptic frame to mean selenographic frame.

$$DCM = \begin{bmatrix} C_\phi C_\psi - C_\theta S_\phi S_\psi & S_\phi C_\psi + C_\theta C_\phi S_\psi & S_\theta S_\psi \\ -C_\phi S_\psi - C_\theta S_\phi C_\psi & -S_\phi S_\psi + C_\theta C_\phi C_\psi & S_\theta C_\psi \\ S_\theta S_\phi & -S_\theta C_\phi & C_\theta \end{bmatrix} \quad (3\text{-}6)$$

5. Complete the transformation using the vector equation

$$\overline{r}_R = [DCM]\overline{r}_E \quad (3\text{-}7)$$

In order to obtain in-plane and out-of-plane control accelerations, a transformation from the rotating frame to RSW frame is required. RSW frame is a spacecraft-fixed coordinate system that moves with the spacecraft, such that the *R* axis always points along the radial vector from the Moon's center to the spacecraft and the *S* axis points in the direction of the spacecraft's velocity vector and is always perpendicular to the *R* axis in the spacecraft's orbit plane. The *W* axis is normal to the orbit plane, the *R* and *S* axis. The transformation from the rotating frame to the RSW frame is similar to the transformation from the ecliptic to the rotating frame.

Figure 3.3 Transformation from Rotating Frame to RSW Frame

This transformation requires three rotations of Ω, i, and θ respectively about the z axis, the x axis resulting after the first rotation and the z axis resulting after the two rotations (see Figure 3.3), the DCM and the transformation vector equation for which are given as

$$DCM = \begin{bmatrix} C_\Omega C_\theta - C_i S_\Omega S_\theta & S_\Omega C_\theta + C_i C_\Omega S_\theta & S_i S_\theta \\ -C_\Omega S_\theta - C_i S_\Omega C_\theta & -S_\Omega S_\theta + C_i C_\Omega C_\theta & S_i C_\theta \\ S_i S_\Omega & -S_i C_\Omega & C_i \end{bmatrix} \tag{3-8}$$

$$\bar{u}_{RSW} = [DCM]\bar{u}_R \tag{3-9}$$

where $\bar{u}_{RSW}$ and $\bar{u}_R$ are inertial control acceleration vectors expressed in RSW frame and rotating frame respectively. Escabal [86, 87] and Vallado [88], describe lunar reference coordinate fames and transformations in detail.

3.2. MODELING PERTURBATIONS

It is impossible to model the actual motion of a spacecraft due to the size and irregular distribution of matter in the Universe. However, depending on the application and allowable tolerance levels; a system boundary can be selected and the scope of uncertainty in a system can be reduced. Accurate modeling of disturbances or perturbations which cause deviations to the actual motion of a spacecraft is a key aspect in deriving the equations of motion. The major sources of perturbations for a spacecraft include the gravitational force from center and neighboring bodies, solar radiation pressure and atmospheric drag. Since the Moon has no atmosphere; no atmospheric drag is present for a lunar orbiter. Gravitational forces from Sun, Earth and nonspherical Moon generate the primary perturbing accelerations that deviate the lunar orbiter from its ideal trajectory. The gravitational field of the Moon is highly irregular and complex to model due to its non spherical shape but the gravitational forces due to the Earth and Sun can be calculated by assuming them as point masses because of their far distance from the lunar orbiter. Although solar radiation pressure is not a major perturbation source, especially for a small spacecraft, it has been modeled to improve the accuracy of the system model.

3.2.1. Perturbations due to Point Mass: The acceleration due to gravitational force 'a_g' from a point mass is given by Newton's Universal law of gravitation as

$$\overline{F}_g = m_o \overline{a}_g = -\frac{G m_b m_o}{r^3}\overline{r} \Rightarrow \overline{a}_g = -\frac{\mu_b}{r^3}\overline{r} \qquad (3\text{-}10)$$

where

F_g is the force on the spacecraft due to point mass; $\overline{r}$ is position vector from the point mass to the spacecraft; the scalar r is the magnitude of vector $\overline{r}$ which represents the distance from the point mass to the spacecraft; m_o is the mass of the spacecraft; μ_b is the gravitational parameter for the point mass which is given by $\mu = Gm$, "G" being the gravitational constant equal to $6.6695\times10^{-20}\,(km^3)/(kg)(\sec^2)$ and "m_b" being the mass of the respective body.

3.2.2. Perturbations due to Nonspherical Moon: A non-spherical potential function 'U' is used to determine the gravitation force acting on a satellite with a given position due to Moon. The gradient $(\bar{\nabla}U)$ computed using the following equations gives the perturbing acceleration caused by the nonspherical shape of Moon on the orbiting satellite.

$$\begin{aligned}\bar{\nabla}U &= \bar{\nabla}_x U + \bar{\nabla}_y U + \bar{\nabla}_z U \\ &= \left(\frac{\partial U}{\partial r}\frac{\partial r}{\partial x} + \frac{\partial U}{\partial \phi}\frac{\partial \phi}{\partial x} + \frac{\partial U}{\partial \lambda}\frac{\partial \lambda}{\partial x}\right)\hat{x} \\ &+ \left(\frac{\partial U}{\partial r}\frac{\partial r}{\partial y} + \frac{\partial U}{\partial \phi}\frac{\partial \phi}{\partial y} + \frac{\partial U}{\partial \lambda}\frac{\partial \lambda}{\partial y}\right)\hat{y} + \left(\frac{\partial U}{\partial r}\frac{\partial r}{\partial z} + \frac{\partial U}{\partial \phi}\frac{\partial \phi}{\partial z} + \frac{\partial U}{\partial \lambda}\frac{\partial \lambda}{\partial z}\right)\hat{z}\end{aligned} \tag{3-11}$$

where

$$\frac{\partial U}{\partial r} = -\frac{\mu_m}{r^2}\sum_{l=2}^{\infty}\sum_{m=0}^{l}\left(\frac{R_m}{r}\right)^l (l+1)P_{l,m}[\sin(\phi)]\times\left\{C_{l,m}\cos(m\lambda) + S_{l,m}\sin(m\lambda)\right\} \tag{3-12}$$

$$\begin{aligned}\frac{\partial U}{\partial \phi} = \frac{\mu_m}{r}\sum_{l=2}^{\infty}\sum_{m=0}^{l}\left(\frac{R_m}{r}\right)^l &\left\{P_{l,m+1}[\sin(\phi)] - m\tan(\phi)P_{l,m}[\sin(\phi)]\right\} \\ &\times\left\{C_{l,m}\cos(m\lambda) + S_{l,m}\sin(m\lambda)\right\}\end{aligned} \tag{3-13}$$

$$\frac{\partial U}{\partial \lambda} = \frac{\mu_m}{r}\sum_{l=2}^{\infty}\sum_{m=0}^{l}\left(\frac{R_m}{r}\right)^l mP_{l,m}[\sin(\phi)]\times\left\{C_{l,m}\cos(m\lambda) + S_{l,m}\sin(m\lambda)\right\} \tag{3-14}$$

where 'r' is position vector of the spacecraft with components (x, y, z) with respect to the defined $(\hat{\mathbf{x}}, \hat{\mathbf{y}}, \hat{\mathbf{z}})$ frame; μ_m is the gravitational parameter for the Moon which is given by $\mu = Gm$, "G" being the gravitational constant equal to $6.6695\times10^{-20}\,(km^3)/(kg)(\sec^2)$ and m_m being the mass of the respective body; R_m is the Moon's mean equatorial radius equal to 1738 km. The scalar r is the distance from the center of Moon to the spacecraft $r = [(x)^2 + (y)^2 + (z)^2]^{1/2}$. The angle ϕ is the satellite's latitude which is $\phi = \sin^{-1}(z/r)$ and λ is the longitude which can be found using $\lambda = \sin^{-1}(y/x)$. The variables l and m specify degree and order of the gravity model respectively. Constants $C_{l,m}$ and $S_{l,m}$ are the

normalizing gravitational coefficients of degree l and order m. $P_{l,m}$ is the associated Legendre function of degree l and order m. Reference [88] describes the standard approach for evaluating $(\bar{\nabla} U)$ and can be referred to for further details.

Note: The 165x165 gravity model [92] derived from the data from the Lunar Prospector Mission has been utilized to simulate and compute the nonspherical lunar gravitational potential field.

3.2.3. Perturbations due to Solar Radiation Pressure: The acceleration due to solar radiation pressure, $\bar{a}_{SRP}$ according to reference [88] is given by

$$\bar{a}_{SRP} = -\frac{P_{SR} C_R A_s}{m} \frac{\bar{r}_{os}}{|\bar{r}_{os}|} \tag{3-15}$$

where $P_{SR} = 4.57829 \times 10^{-3}\ {kg}/{km.s^2}$; C_R is constant that represents the reflectivity of the exposed material such $0 \le C_R \le 2$. A C_R of 0.0 indicates a perfectly translucent material while a C_R of 1.0 and 2.0 indicates a perfectly absorbent and reflective material respectively. A_r represents the area of the satellite exposed to solar radiations; m is the mass of the spacecraft and $\bar{r}_{os}$ is the vector from the spacecraft to the center of the Sun.

The following conditions are checked for shadowing [91]:

$$\bar{r}_{mo}.\bar{r}_{ms} < 0 \quad \text{and}$$

$$|\bar{r}_{mo}| \sin\left[\cos^{-1}\frac{\bar{r}_{mo}.\bar{r}_{ms}}{|\bar{r}_{mo}|}\right] < R_m \tag{3-16}$$

In these inequalities, R_p is the radius of the Moon; $\bar{r}_{mo}$ is the vector from the center of the Moon to the spacecraft and $\bar{r}_{mo}$ is the vector from the center of the Moon to the center of the Sun. If the spacecraft is in shadow of the center body then the acceleration due to solar radiation pressure is zero.

3.3. EQUATIONS OF MOTION

The equations of motion for a spacecraft orbiting the Moon have been derived in this section. Subscript *s, e, m, o* are used to denote the Sun, the Earth, the Moon, and the lunar orbiter respectively. Figure 3.4 describes the geometry of the four bodies involved in this problem. Thus, $\overline{R}_s, \overline{R}_e, \overline{R}_m$ and $\overline{R}_o$ are vectors from the origin of inertial frame to the center of Sun, Earth, the Moon and the lunar orbiter respectively.

Figure 3.4 Basic Geometry of the Four Bodies Involved

The vectors $\overline{r}_{se}$ is therefore the vector from the center of the Sun to the center of the Earth; $\overline{r}_{sm}$ is the vector from the center of the Sun to the center of the Moon; $\overline{r}_{so}$ is the vector from the center of the Sun to the lunar orbiter; $\overline{r}_{em}$ is the vector from the center of Earth to the center of the Moon; $\overline{r}_{eo}$ is the vector from the center of the Earth to the center of the lunar orbiter; $\overline{r}_{mo}$ is the vector from the center of the Moon to the center of the lunar orbiter, such that

$$\overline{r}_{eo} = \overline{r}_{em} + \overline{r}_{mo} \tag{3-17}$$

$$\overline{r}_{so} = -\overline{r}_{es} + \overline{r}_{em} + \overline{r}_{mo} \tag{3-18}$$

$$\overline{r}_{sm} = -\overline{r}_{es} + \overline{r}_{em} \tag{3-19}$$

The vectors $\overline{r}_{em}$ and $\overline{r}_{se}$ can easily be found using ephemerides data and equations available in reference [86, 87, 88]. $\overline{r}_{mo}$ represents the position vector of the spacecraft with respect to the inertial frame and it depends on the spacecraft's initial orbital elements and can propagated to future times using the nonlinear equations of motion derived in this section.

Combining Newton's second law of motion and Newton's law of gravitation, the sum of forces acting on the Moon, F_m and the spacecraft, F_o defined with respect to the inertial frame, can individually be written as

$$F_m = m_m \ddot{\overline{R}}_m = -\frac{G m_s m_m}{r_{sm}^3}\overline{r}_{sm} - \frac{G m_e m_m}{r_{em}^3}\overline{r}_{em} \tag{3-20}$$

$$F_o = m_o \ddot{\overline{R}}_o = -\frac{G m_s m_o}{r_{so}^3}\overline{r}_{so} - \frac{G m_e m_o}{r_{eo}^3}\overline{r}_{eo} + m_o \overline{\nabla} U_m + m_o \overline{a}_{SRP} + m_o \overline{u} \tag{3-21}$$

The nonlinear equations of motion describing the perturbed motion of the spacecraft relative to the Moon defined with respect to the inertial frame can be obtained by subtracting eqn. (3-20) from eqn. (3-21) since $\ddot{\overline{r}}_{mo} = \ddot{\overline{R}}_o - \ddot{\overline{R}}_m$, as

$$\ddot{\overline{r}}_{mo} = -\frac{\mu_e}{r_{eo}^3}\overline{r}_{eo} - \frac{\mu_s}{r_{so}^3}\overline{r}_{so} + \overline{\nabla} U_m + \overline{a}_{SRP} + \frac{\mu_e}{r_{em}^3}\overline{r}_{em} + \frac{\mu_s}{r_{sm}^3}\overline{r}_{sm} + \overline{u} \tag{3-22}$$

which can be written in Cartesian form [89] and with respect to the rotating frame (after using the rotation as explained in Section 3.1) as

$$\ddot{x} = 2\omega_m \dot{y} + \omega_m{}^2 x - \mu_e \frac{(r_{em_x} + x)}{[(r_{em_x} + x)^2 + (r_{em_y} + y)^2 + (r_{em_z} + z)^2]^{3/2}}$$
$$- \bar{\nabla}_x U + \bar{a}_{SRP_X} + \mu_s \frac{(r_{es_x} - r_{em_x} - x)}{[(r_{es_x} - r_{em_x} - x)^2 + (r_{es_y} - r_{em_y} - y)^2 + (r_{es_z} - r_{em_z} - z)^2]^{3/2}}$$
$$+ \mu_e \frac{r_{em_x}}{[(r_{em_x})^2 + (r_{em_y})^2 + (r_{em_z})^2]^{3/2}} + \mu_s \frac{(r_{sm_x})}{[(r_{sm_x})^2 + (r_{sm_y})^2 + (r_{sm_z})^2]^{3/2}} + u_x$$

(3-23)

$$\ddot{y} = -2\omega_m \dot{x} + \omega_m{}^2 y - \mu_e \frac{(r_{em_y} + y)}{[(r_{em_x} + x)^2 + (r_{em_y} + y)^2 + (r_{em_z} + z)^2]^{3/2}}$$
$$- \bar{\nabla}_y U + \bar{a}_{SRP_Y} + \mu_s \frac{(r_{es_y} - r_{em_y} - y)}{[(r_{es_x} - r_{em_x} - x)^2 + (r_{es_y} - r_{em_y} - y)^2 + (r_{es_z} - r_{em_z} - z)^2]^{3/2}}$$
$$+ \mu_e \frac{r_{em_y}}{[(r_{em_x})^2 + (r_{em_y})^2 + (r_{em_z})^2]^{3/2}} + \mu_s \frac{(r_{sm_y})}{[(r_{sm_x})^2 + (r_{sm_y})^2 + (r_{sm_z})^2]^{3/2}} + u_y$$

(3-24)

$$\ddot{z} = -\mu_e \frac{(r_{em_z} + z)}{[(r_{em_x} + x)^2 + (r_{em_y} + y)^2 + (r_{em_z} + z)^2]^{3/2}}$$
$$+ \mu_s \frac{(r_{es_z} - r_{em_z} - z)}{[(r_{es_x} - r_{em_x} - x)^2 + (r_{es_y} - r_{em_y} - y)^2 + (r_{es_z} - r_{em_z} - z)^2]^{3/2}}$$
$$- \bar{\nabla}_z U + \bar{a}_{SRP_Z} + \mu_e \frac{r_{em_z}}{[(r_{em_x})^2 + (r_{em_y})^2 + (r_{em_z})^2]^{3/2}} + \mu_s \frac{(r_{sm_z})}{[(r_{sm_x})^2 + (r_{sm_y})^2 + (r_{sm_z})^2]^{3/2}} + u_z$$

(3-25)

where (x, y, z) is position of the spacecraft with respect to the rotating $(\hat{\mathbf{x}}, \hat{\mathbf{y}}, \hat{\mathbf{z}})$ frame; $\mu_s, \mu_e \text{ and } \mu_m$ is the gravitational parameter for the Sun, Earth and Moon respectively which is given by $\mu = Gm$, G being the gravitational constant equal to $6.6695 \times 10^{-20} (km^3)/(kg)(\sec^2)$ and m being the mass of the respective body; u_x, u_y and u_z are coordinates of the control acceleration vector $\bar{u}$; $(r_{em_x}, r_{em_y}, r_{em_z})$ are coordinates of $\bar{r}_{em}$ which

is the vector from the center of the Earth to the center of the Moon; $(r_{es_x}, r_{es_y}, r_{es_z})$ are coordinates of $\bar{r}_{es}$ which is the vector from the Earth to the Sun; $(r_{sm_x}, r_{sm_y}, r_{sm_z})$ are coordinates of $\bar{r}_{sm}$ which is the vector from the Sun to the Moon. The vector $(\bar{\nabla} U)$ is the gradient of the non-spherical gravitational potential function for the Moon, U as defined in Section 3.2.2.

3.4. SIMULATIONS WITH NO CONTROL INPUT

Now that a mathematical model describing the nonlinear dynamics of the spacecraft in a lunar orbit perturbed by gravity fields of the nonspherical Moon, Earth, and Sun, and solar radiation pressure, has been derived, it is essential to study the effect of these perturbations to justify if orbit control is even necessary. In this section, the effect of perturbations on a spacecraft in various lunar orbits is evaluated. This is done by simulating the changes in orbital elements of spacecraft in a low altitude lunar orbit (suitable for mapping), a high-altitude inclined elliptical frozen orbit, and a high altitude circular polar orbit (suitable for communication), with no control thrust applied. Orbits A, B and C (see Figure 3.5) are simulated and histories of orbital elements are plotted with time. Orbit A represents a good choice of the initial orbit for Sun-synchronous mapping. Orbit B represents the most recommended choice for lunar communication by NASA. Orbit C represents the initial orbit of the proposed option for lunar communication in this thesis, i.e. a geo-synchronous orbit.

Orbital Elements	Orbit A: Low-altitude circular polar orbit	Orbit B: High-altitude Frozen orbit [25]	Orbit B: High-altitude polar orbit
Semimajor axis	1838 km	6142.4 km	10000 km
Eccentricity	0.001	0.6	0.001
Inclination	90 deg	57.7 deg	90 deg
Right Ascension of ascending node	45 deg	0 deg	90 deg
Argument of periapsis	270 deg	90 deg	90 deg

Figure 3.5 Initial Orbital Elements of Orbits Simulated with No Control

Note: For all numerical simulation and analysis the degree $l_{\max} = 25$ and the order $m_{\max} = 25$ is selected [76]. Also, the simulation history of true anomaly is not shown as it mainly represents the angular motion of spacecraft in its orbit.

The six plots presented as Figure 3.6 show the changes in the inertial classical orbital elements and periapsis altitude with time of a spacecraft orbiting the Moon in Orbit A. No control thrust is applied and the effect of perturbations on the spacecraft's orbit is illustrated in this figure. In all these plots, the trajectory in red represents the actual motion of the spacecraft, while the blue line represents the initial orbital element. It can be seen that the perturbations tend to increase the eccentricity of the orbit making it non-circular. The peripasis altitude starts to decrease drastically with a decline in altitude of about 60 km in just 90 days. This indicates that the operational lifetime (the time period that the spacecraft stays above the lunar surface without impact) of spacecraft in Orbit A would only be a few months. The plot of ascending node shows a decrease in ascending node by 1 deg every 45 days. However, for Sun-synchronous lunar mapping, the desired rate of change of ascending node is an increase of 1 deg per day.

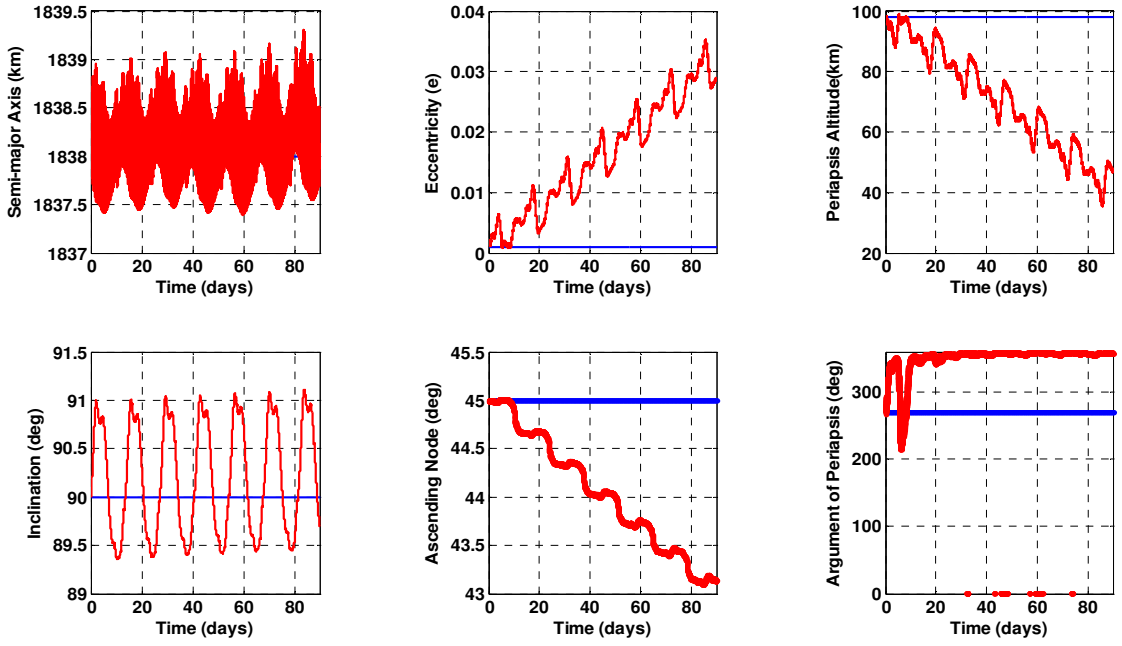

Figure 3.6 Inertial Orbital Elements of Uncontrolled Spacecraft in Orbit A

For a high altitude orbit, the margins of acceptable errors in the state are high, since the periapsis altitude must decrease greatly due to initial high altitude before impacting the lunar surface. The oscillating effects of the perturbations on the inertial classical orbital elements and periapsis altitude of a spacecraft in Orbit B, as seen in Figure 3.7, tend to keep them within acceptable regions. Thus, the frozen Orbit B offers a long operational lifetime with few impulse maneuvers. However, the apoapsis of the spacecraft remains nearly fixed with respect to the inertial frame, but it rotates with respect to the rotating frame (see Figure 3.8). This happens because the $\hat{\mathbf{x}}$ unit vector, which is always pointing towards the center of the Earth, rotates as the Moon revolves around the Earth.

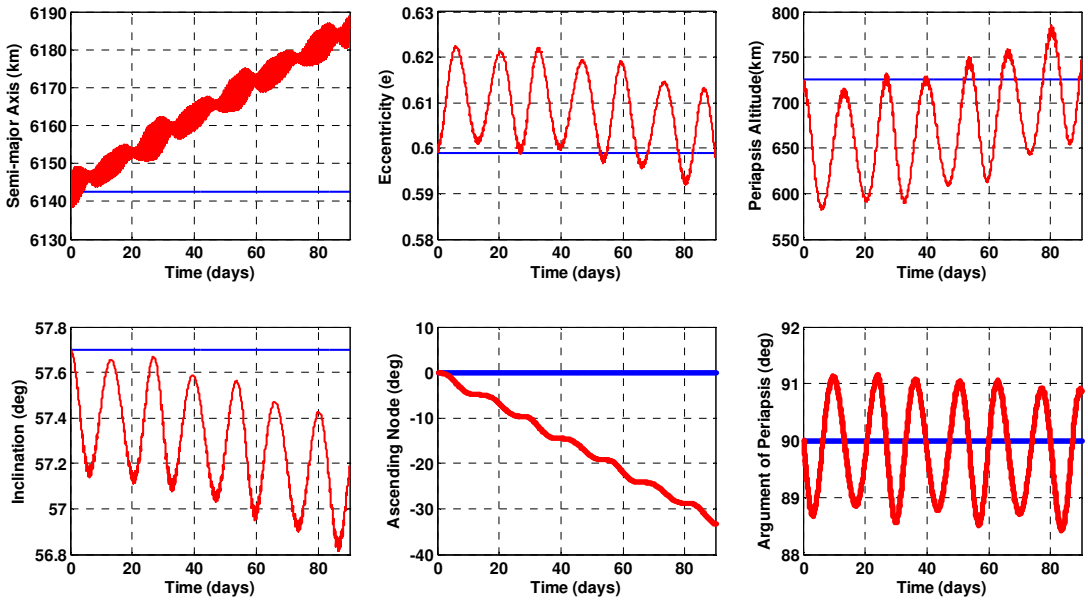

Figure 3.7 Inertial Orbital Elements of Uncontrolled Spacecraft in Orbit B

The rotation of the orbit plane with respect to Earth results in drastic changes in the far side coverage capability of constellations with inclined frozen orbits. To avoid this, the orbit needs to be fixed with respect to the rotating frame, which is possible if a continuous change in the ascending node is provided at the rate at which the Moon revolves around the Earth i.e. $\dot{\Omega} = \omega_m$ = 2.661699 x 10-6 rad/sec.

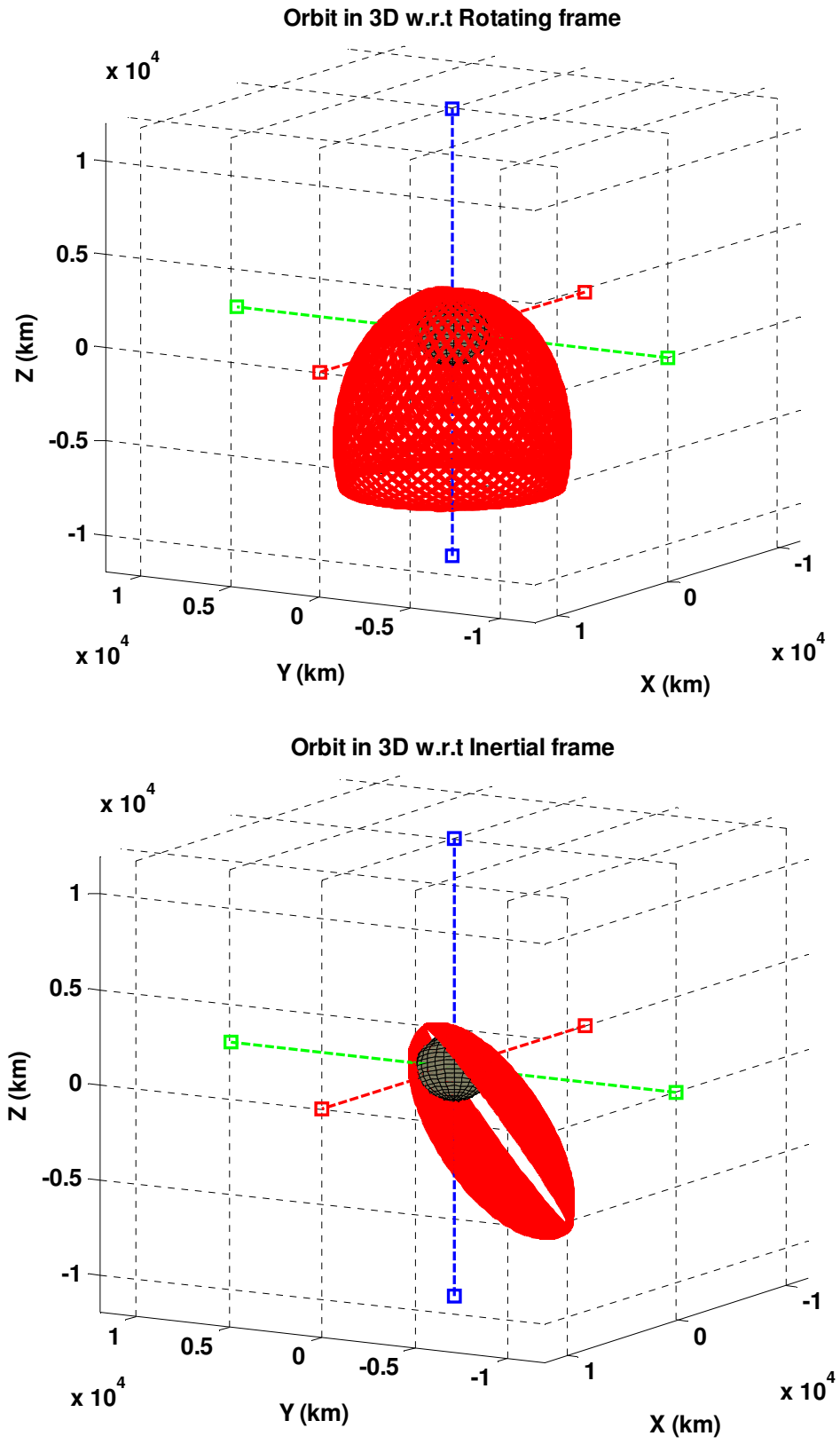

Figure 3.8 Three Dimensional Visualization of Orbit B Simulated with No Control

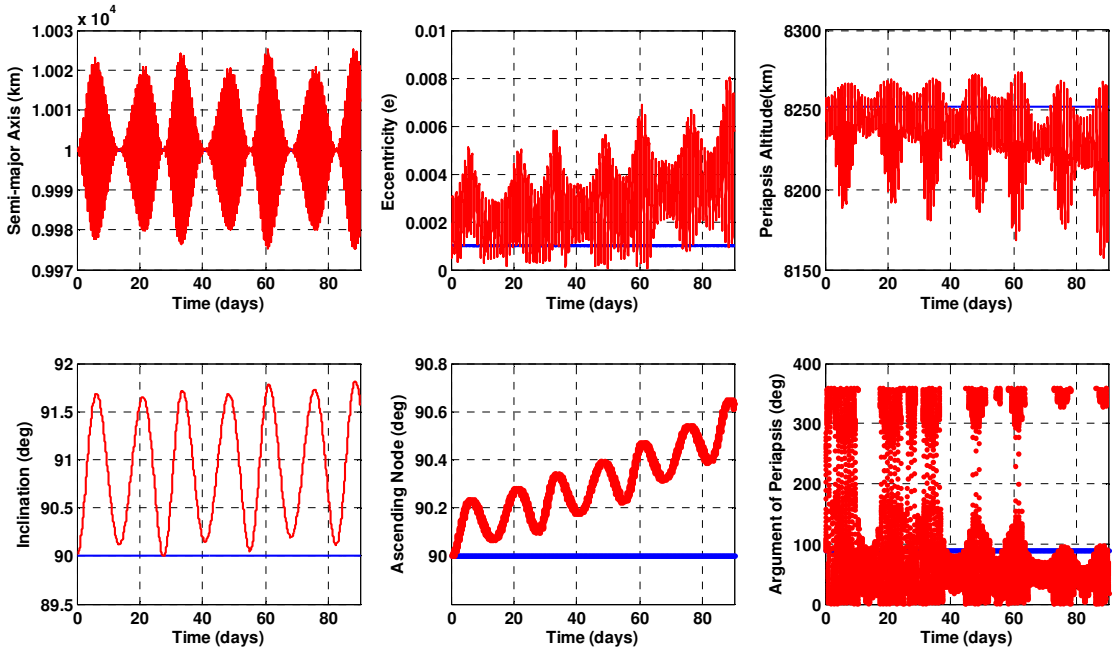

Figure 3.9 Inertial Orbital Elements of Uncontrolled Spacecraft in Orbit C

Figure 3.9 shows the change in orbital elements for Orbit C, which is a suitable choice for geo-synchronous lunar constellations. It is evident from the ascending node plots that the lunar gravity field is not capable of producing a Sun-synchronous or a geo-synchronous change in ascending node.

These simulation results, thus confirm that in order to provide the change in orbit plane desired for Sun-synchronous mapping and geo-synchronous communication; and to simultaneously control the spacecraft's altitude, eccentricity, and inclination, it is essential to apply continuous control. In the next section, a nonlinear control technique is presented; this technique is used to compute minimal control accelerations (which in turn would lead to low-thrust) required to maintain the spacecraft in desired lunar orbits.

4. CONTROLLER DESIGN

Once the nonlinear equations describing the dynamics of the spacecraft have been obtained, the motion of the spacecraft can be controlled using the State Dependent Riccati Equation (SDRE) approach (Cloutier et al., [83, 84]). This approach involves converting the nonlinear dynamics of the problem into a linear-like form and then using a feedback control law to obtain the desired effect.

4.1. GENERAL DESCRIPTION OF THE SDRE CONTROL TECHNIQUE

In this section, the control technique that is used to find continuous control accelerations, to control the motion of a spacecraft is described. To better understand this approach; a nonlinear dynamic system is assumed for which, the state-space model can be written as

$$\dot{x} = f(x) + g(x)u. \tag{4-1}$$

where $x \in R^n, u \in R^m, f(x) \in C^k, g(x) \in C^k, k \geq 1$

The SDRE approach [71] provides a framework to obtain suboptimal feedback control of autonomous, infinite-horizon, nonlinear quadratic regulator problems. The objective of such control problems is to find the feedback control *u(x)* that minimizes the quadratic performance index, which can be defined in the state dependent form as

$$J = \frac{1}{2}\int_{t_0}^{\infty} [x^T Q(x)x + u^T R(x)u]dt \tag{4-2}$$

where the terms *Q(x)* and *R(x)* are state dependent weighting matrices. These matrices provide a trade-off between state *x* and control *u,* and can be chosen depending on the desired performance objective. To ensure local stability, it is essential to make sure that the matrix *Q(x)* is positive semidefinite for all x i.e. $Q(x) \geq 0$; and the matrix *R(x)* is required to be positive definite for all *x* i.e. *R(x)>0*.

The first step in using the SDRE approach is to convert the state space model of the nonlinear system into a state dependent coefficient form, which is defined by the following linear structure

$$\dot{x} = A(x)x + B(x)u \tag{4-3}$$

such that $f(x) = A(x)x$ and $g(x) = B(x)$

It is required that pair$\{A(x), B(x)\}$ be pointwise stabilizable in a linear sense for all *x.* This can be insured by checking the controllability matrix for full rank [67]. Once the linear state dependent coefficient form has been obtained, the frozen state dependent algebraic Riccati equation

$$A^T(x)P(x) + P(x)A(x) - P(x)B(x)R^{-1}(x)B^T(x)P(x) + Q(x) = 0 \tag{4-4}$$

can be solved to obtain a positive definite state dependent matrix *P(x).* The matrix *P(x)* obtained can then be used to calculate the necessary control, *u*, using the nonlinear feedback control law

$$u = -R^{-1}(x)B^T(x)P(x)x = -K(x)x, \text{ where } K(x) = R^{-1}(x)B^T(x)P(x) \tag{4-5}$$

This control law is locally stable and optimal with respect to the infinite time performance index [6]. The challenging aspect of this control approach is the solution of the state dependent Riccati equation which is difficult to obtain in general but can easily be obtained numerically. In order to achieve state tracking or command following, the SDRE approach can be implemented as a servomechanism [83, 85]. The SDRE feedback control law for servo control is given by

$$u = -R^{-1}(x)B^T(x)P(x)(x - x_R) = -K(x)(x - x_R) \tag{4-6}$$

where it desired for state variables x to track the reference state x_R.

4.2. CONTROL FORMULATION EMPLOYING SDRE TECHNIQUE

The SDRE approach described in the last section is followed to design a controller for control the motion of a spacecraft orbiting the Moon. First, a state vector for the spacecraft is defined as

$$X = \begin{bmatrix} x & y & z & \dot{x} & \dot{y} & \dot{z} \end{bmatrix}^T \tag{4-7}$$

for which the nonlinear dynamic equations (3-22) to (3-25) apply. The variables x, y, z and $\dot{x}, \dot{y}, \dot{z}$ in the state vector represent the position and velocity of the spacecraft with respect to the rotating $(\hat{\mathbf{x}}, \hat{\mathbf{y}}, \hat{\mathbf{z}})$ frame. The nonlinear equations of motion of spacecraft can then be written in the state-space form as

$$x_1 = x \tag{4-8}$$

$$x_2 = y \tag{4-9}$$

$$x_3 = z \tag{4-10}$$

$$\dot{x}_1 = x_4 = \dot{x} \tag{4-11}$$

$$\dot{x}_2 = x_5 = \dot{y} \tag{4-12}$$

$$\dot{x}_3 = x_6 = \dot{z} \tag{4-13}$$

$$\begin{aligned} \dot{x}_4 = {} & 2\omega_m x_5 + \omega_m{}^2 x_1 - \mu_e \frac{(r_{em_x} + x_1)}{[(r_{em_x} + x_1)^2 + (r_{em_y} + x_2)^2 + (r_{em_z} + x_3)^2]^{3/2}} \\ & - \bar{\nabla}_x U + \mu_s \frac{(r_{es_x} - r_{em_x} - x_1)}{[(r_{es_x} - r_{em_x} - x_1)^2 + (r_{es_y} - r_{em_y} - x_2)^2 + (r_{es_z} - r_{em_z} - x_3)^2]^{3/2}} \\ & + \mu_e \frac{r_{em_x}}{[(r_{em_x})^2 + (r_{em_y})^2 + (r_{em_z})^2]^{3/2}} + \mu_s \frac{(r_{sm_x})}{[(r_{sm_x})^2 + (r_{sm_y})^2 + (r_{sm_z})^2]^{3/2}} + u_x \end{aligned} \tag{4-14}$$

$$\dot{x}_5 = -2\omega_m x_4 + \omega_m{}^2 x_2 - \mu_e \frac{(r_{em_y} + x_2)}{[(r_{em_x} + x)^2 + (r_{em_y} + x_2)^2 + (r_{em_z} + x_3)^2]^{3/2}}$$
$$-\bar{\nabla}_y U + \mu_s \frac{(r_{es_y} - r_{em_y} - x_2)}{[(r_{es_x} - r_{em_x} - x_1)^2 + (r_{es_y} - r_{em_y} - x_2)^2 + (r_{es_z} - r_{em_z} - x_3)^2]^{3/2}} \quad (4\text{-}15)$$
$$+\mu_e \frac{r_{em_y}}{[(r_{em_x})^2 + (r_{em_y})^2 + (r_{em_z})^2]^{3/2}} + \mu_s \frac{(r_{sm_y})}{[(r_{sm_x})^2 + (r_{sm_y})^2 + (r_{sm_z})^2]^{3/2}} + u_y$$

$$\dot{x}_6 = -\bar{\nabla}_z U - \mu_e \frac{(r_{em_z} + x_3)}{[(r_{em_x} + x_1)^2 + (r_{em_y} + x_2)^2 + (r_{em_z} + x_3)^2]^{3/2}}$$
$$+\mu_s \frac{(r_{es_z} - r_{em_z} - x_3)}{[(r_{es_x} - r_{em_x} - x_1)^2 + (r_{es_y} - r_{em_y} - x_2)^2 + (r_{es_z} - r_{em_z} - x_3)^2]^{3/2}} \quad (4\text{-}16)$$
$$+\mu_e \frac{r_{em_z}}{[(r_{em_x})^2 + (r_{em_y})^2 + (r_{em_z})^2]^{3/2}} + \mu_s \frac{(r_{sm_z})}{[(r_{sm_x})^2 + (r_{sm_y})^2 + (r_{sm_z})^2]^{3/2}} + u_z$$

Now that the nonlinear spacecraft dynamics is in state-space form, it must be converted into a linear-like state coefficient form. This is necessary to obtain the *A(x)* and *B(x)* matrices that are used to solve the Riccati equation.

The state coefficient form for this control problem is obtained as

$$\dot{X} = A(X)X + B(X)u \quad (4\text{-}17)$$

with the matrices *A(X)* and *B(X)* defined as

$$A(X) = \begin{bmatrix} 0 & 0 & 0 & 1 & 0 & 0 \\ 0 & 0 & 0 & 0 & 1 & 0 \\ 0 & 0 & 0 & 0 & 0 & 1 \\ a_{41} & 0 & 0 & 0 & 2\omega_m & 0 \\ 0 & a_{52} & 0 & -2\omega_m & 0 & 0 \\ 0 & 0 & a_{63} & 0 & 0 & 0 \end{bmatrix}, \text{ and } \quad B(X) = \begin{bmatrix} 0 & 0 & 0 \\ 0 & 0 & 0 \\ 0 & 0 & 0 \\ 1 & 0 & 0 \\ 0 & 1 & 0 \\ 0 & 0 & 1 \end{bmatrix}$$

where the terms a_{41}, a_{52}, and a_{63} are given by

$$a_{41} = \omega_m{}^2 - \frac{\mu_e}{x_1}\frac{(r_{em_x}+x_1)}{[(r_{em_x}+x_1)^2+(r_{em_y}+x_2)^2+(r_{em_z}+x_3)^2]^{3/2}} - \frac{\bar{\nabla}_x U}{x_1}$$
$$+\frac{\mu_s}{x_1}\frac{(r_{es_x}-r_{em_x}-x_1)}{[(r_{es_x}-r_{em_x}-x_1)^2+(r_{es_y}-r_{em_y}-x_2)^2+(r_{es_z}-r_{em_z}-x_3)^2]^{3/2}}$$
$$+\frac{\mu_e}{x_1}\frac{r_{em_x}}{[(r_{em_x})^2+(r_{em_y})^2+(r_{em_z})^2]^{3/2}}+\frac{\mu_s}{x_1}\frac{(r_{sm_x})}{[(r_{sm_x})^2+(r_{sm_y})^2+(r_{sm_z})^2]^{3/2}}$$

$$a_{52} = \omega_m{}^2 - \frac{\mu_e}{x_2}\frac{(r_{em_y}+x_2)}{[(r_{em_x}+x)^2+(r_{em_y}+x_2)^2+(r_{em_z}+x_3)^2]^{3/2}} - \frac{\bar{\nabla}_y U}{x_2}$$
$$+\frac{\mu_s}{x_2}\frac{(r_{es_y}-r_{em_y}-x_2)}{[(r_{es_x}-r_{em_x}-x_1)^2+(r_{es_y}-r_{em_y}-x_2)^2+(r_{es_z}-r_{em_z}-x_3)^2]^{3/2}}$$
$$+\frac{\mu_e}{x_2}\frac{r_{em_y}}{[(r_{em_x})^2+(r_{em_y})^2+(r_{em_z})^2]^{3/2}}+\frac{\mu_s}{x_2}\frac{(r_{sm_y})}{[(r_{sm_x})^2+(r_{sm_y})^2+(r_{sm_z})^2]^{3/2}}$$

$$a_{63} = -\frac{\mu_e}{x_3}\frac{(r_{em_z}+x_3)}{[(r_{em_x}+x_1)^2+(r_{em_y}+x_2)^2+(r_{em_z}+x_3)^2]^{3/2}} - \frac{\bar{\nabla}_z U}{x_3}$$
$$+\frac{\mu_s}{x_3}\frac{(r_{es_z}-r_{em_z}-x_3)}{[(r_{es_x}-r_{em_x}-x_1)^2+(r_{es_y}-r_{em_y}-x_2)^2+(r_{es_z}-r_{em_z}-x_3)^2]^{3/2}}$$
$$+\frac{\mu_e}{x_3}\frac{r_{em_z}}{[(r_{em_x})^2+(r_{em_y})^2+(r_{em_z})^2]^{3/2}}+\frac{\mu_s}{x_3}\frac{(r_{sm_z})}{[(r_{sm_x})^2+(r_{sm_y})^2+(r_{sm_z})^2]^{3/2}} \qquad (4\text{-}18)$$

The state and control weights are heuristically chosen depending on the kind of lunar orbit, allowable state errors and desired control trajectory, and take the form

$$\mathbf{Q} = diag\{q_{11}, q_{22}, q_{33}, q_{44}, q_{55}, q_{66}\} \text{ and } \mathbf{R} = diag\{r_{11}, r_{22}, r_{33}\}$$

After obtaining the *A(X), B(X), Q(X),* and *R(X)* matrices, the state dependent algebraic Riccati equation can be solved to obtain *P(X)* and then the control *u(X)* can finally be calculated using the servo control law as described in the last section through

$$u = -K(X)[X - X_{ref}] \; where \; K(X) = -R^{-1}(X)B^{T}(X)P(X) \qquad (4\text{-}19)$$

where X_{ref} is the state elements of the reference or desired orbit. X_{ref} is found by converting the reference classical orbital elements to Cartesian form [89]. X_{ref} is propagated by updating the classical orbital elements of the reference orbit at every time step. The true anomaly is updated using Kepler's equation [88]. Other orbital elements can be updated at the desired rate, depending on the orbit desired after control thrust has been applied. For example, the X_{ref} for a Sun-synchronous orbit is obtained by updating the ascending node each time step at a Sun-synchronous rate of $\dot{\Omega} = 0.9856 \text{ deg per day}$.

Note: The terms a_{41}, a_{52} and a_{63} are not defined when x_1, x_2 and x_3 are zero respectively. This happens when the spacecraft is within or crossing the *x*-*y* plane (lunar equatorial plane), *x*-*z* plane and the *y*-*z* plane. x_1 is near zero when the spacecraft is near or within the rotating *y*-*z* plane, which for a polar orbit corresponds to an ascending node of 90 deg or 270 deg measured with respect to the rotating frame. Similarly, x_2 is near zero when the spacecraft is near or within the rotating *x*-*z* plane, which for a polar orbit corresponds to an ascending node of 0 deg or 180 deg measured with respect to the rotating frame. For an orbit with near equatorial (0 deg) inclination, x_3 will always be near zero. Cases with two coordinates simultaneously zero occur when the spacecraft crosses either of the rotating axis i.e. *x*-axis or *y*-axis or *z*-axis. Like x_1 and x_2 both are near zero, when the spacecraft is crossing the poles i.e. the *z*-axis. These situations result in an undefined *A(X)* matrix which causes numerical integration errors and is responsible for very large or infinite control magnitude. To avoid this, the choice of *A(X)* matrix can be changed whenever x_1 or x_2 or x_3 is near zero. For example, in cases when only x_1 is zero, the *A(X)* matrix can be changed to

$$A_N(X) = \begin{bmatrix} 0 & 0 & 0 & 1 & 0 & 0 \\ 0 & 0 & 0 & 0 & 1 & 0 \\ 0 & 0 & 0 & 0 & 0 & 1 \\ \omega_m{}^2 & a_{42_N} & 0 & 0 & 2\omega_m & 0 \\ 0 & a_{52} & 0 & -2\omega_m & 0 & 0 \\ 0 & 0 & a_{63} & 0 & 0 & 0 \end{bmatrix}, \text{ with}$$

$$a_{42_N} = -\frac{\mu_e}{x_2}\frac{(r_{em_x}+x_1)}{[(r_{em_x}+x_1)^2+(r_{em_y}+x_2)^2+(r_{em_z}+x_3)^2]^{3/2}} - \frac{\bar{\nabla}_x U}{x_2}$$
$$+\frac{\mu_s}{x_2}\frac{(r_{es_x}-r_{em_x}-x_1)}{[(r_{es_x}-r_{em_x}-x_1)^2+(r_{es_y}-r_{em_y}-x_2)^2+(r_{es_z}-r_{em_z}-x_3)^2]^{3/2}}$$
$$+\frac{\mu_e}{x_2}\frac{r_{em_x}}{[(r_{em_x})^2+(r_{em_y})^2+(r_{em_z})^2]^{3/2}}+\frac{\mu_s}{x_2}\frac{(r_{sm_x})}{[(r_{sm_x})^2+(r_{sm_y})^2+(r_{sm_z})^2]^{3/2}}$$

Similarly, when x_1 and x_2 are both near zero, the *A(X)* can be changed to

$$A_N(X) = \begin{bmatrix} 0 & 0 & 0 & 1 & 0 & 0 \\ 0 & 0 & 0 & 0 & 1 & 0 \\ 0 & 0 & 0 & 0 & 0 & 1 \\ \omega_m{}^2 & 0 & a_{43_N} & 0 & 2\omega_m & 0 \\ 0 & \omega_m{}^2 & a_{53_N} & -2\omega_m & 0 & 0 \\ 0 & 0 & a_{63} & 0 & 0 & 0 \end{bmatrix}, \text{ with}$$

$$a_{43_N} = -\frac{\mu_e}{x_3}\frac{(r_{em_x}+x_1)}{[(r_{em_x}+x_1)^2+(r_{em_y}+x_2)^2+(r_{em_z}+x_3)^2]^{3/2}} - \frac{\bar{\nabla}_x U}{x_3}$$
$$+\frac{\mu_s}{x_3}\frac{(r_{es_x}-r_{em_x}-x_1)}{[(r_{es_x}-r_{em_x}-x_1)^2+(r_{es_y}-r_{em_y}-x_2)^2+(r_{es_z}-r_{em_z}-x_3)^2]^{3/2}}$$
$$+\frac{\mu_e}{x_3}\frac{r_{em_x}}{[(r_{em_x})^2+(r_{em_y})^2+(r_{em_z})^2]^{3/2}}+\frac{\mu_s}{x_3}\frac{(r_{sm_x})}{[(r_{sm_x})^2+(r_{sm_y})^2+(r_{sm_z})^2]^{3/2}}, \text{ and}$$

$$a_{53_N} = -\frac{\mu_e}{x_3}\frac{(r_{em_y}+x_2)}{[(r_{em_x}+x)^2+(r_{em_y}+x_2)^2+(r_{em_z}+x_3)^2]^{3/2}} - \frac{\bar{\nabla}_y U}{x_3}$$
$$+\frac{\mu_s}{x_3}\frac{(r_{es_y}-r_{em_y}-x_2)}{[(r_{es_x}-r_{em_x}-x_1)^2+(r_{es_y}-r_{em_y}-x_2)^2+(r_{es_z}-r_{em_z}-x_3)^2]^{3/2}}$$
$$+\frac{\mu_e}{x_3}\frac{r_{em_y}}{[(r_{em_x})^2+(r_{em_y})^2+(r_{em_z})^2]^{3/2}}+\frac{\mu_s}{x_3}\frac{(r_{sm_y})}{[(r_{sm_x})^2+(r_{sm_y})^2+(r_{sm_z})^2]^{3/2}}$$

When not dealing with polar orbits that correspond to an ascending node of 0, 90, 180 or 270 deg (measured with respect to the rotating frame), and equatorial orbits, the time period when x_1, x_2 *or* x_3 is near zero is very short. For such cases, a way around using different choices of *A(X)* is to not compute the gain matrix *K,* when x_1, x_2 and x_3 are near zero and instead use the *K* obtained when x_1, x_2 and x_3 were last near zero. This is also true when dealing with orbits with high perturbation effects.

5. NUMERICAL RESULTS AND SIMULATION

In this section, the simulation results obtained after the application of the nonlinear continuous control strategy discussed in the last section, to maintain spacecraft in Sun-synchronous and geo-synchronous lunar orbits, are presented and discussed. The feasibility of electric propulsion for continuous control of spacecraft in these orbits is determined by examining if the current state of electric propulsion hardware can provide the required levels of control accelerations computed by the SDRE-based controller. Orbits are simulated for a time period more than one full lunar ephemeris with respect to Earth (27.32 days), so that a better understanding on the behavior of controlled orbits can be obtained and all possible cases can be included.

5.1. SIMULATIONS WITH CONTINUOUS CONTROL INPUT

The first group of simulations performed involved maintaining the spacecraft in a low altitude Sun-synchronous lunar orbit suitable for mapping. To do this the spacecraft was assumed to have been inserted into a lunar orbit such that its initial nominal orbit is defined by orbital elements of Orbit A (see Figure 3.5). Considering an unperturbed propagation of Orbit A as the reference orbit with its ascending node (measured with respect to the inertial frame) increasing at a Sun-synchronous rate of 0.9856 deg per day, the SDRE controller designed was applied to control the perturbed motion of the spacecraft such that its actual motion follows the reference orbit. The results obtained after performing short (few orbit revolutions) and long term (one month) simulations of the controlled spacecraft in Orbit A are presented in Figures 5.1 to 5.4. For these simulations the control gains are computed using the state error and control weights

$$Q_A = \begin{bmatrix} 0.005 & 0 & 0 & 0 & 0 & 0 \\ 0 & 0.005 & 0 & 0 & 0 & 0 \\ 0 & 0 & 0.005 & 0 & 0 & 0 \\ 0 & 0 & 0 & 0.05 & 0 & 0 \\ 0 & 0 & 0 & 0 & 0.05 & 0 \\ 0 & 0 & 0 & 0 & 0 & 0.05 \end{bmatrix}, \text{and } R_A = \begin{bmatrix} 5\times10^8 & 0 & 0 \\ 0 & 5\times10^8 & 0 \\ 0 & 0 & 5\times10^8 \end{bmatrix}$$

The state error and control weight matrices, *Q(X)* and *R(X)* are chosen to not be a function of the state vector. To obtain least feasible levels of control, the diagonal matrix elements of *R(X)* are given high values and that of *Q(X)* are given low values. The changes in the inertial classical orbital elements and the radius of periapsis of the controlled spacecraft plotted against time can be observed in Figure 5.1 and 5.3. In all these plots, the trajectory in red represents the actual motion of the controlled spacecraft; while the one in blue represents the reference orbit i.e. the desired motion of the spacecraft. The deviations of the controlled orbit from the reference orbit, as seen in these graphs, are very small and tend to follow a repetitive cyclic pattern with time. A maximum error of only about 0.02 deg is seen in the Sun-synchronous ascending node tracking and that in inclination is about 0.0012 deg. It can be seen that the radius of periapsis remains within a 1.2 km range from the reference offering a spacecraft operational lifetime that is not affected by orbit perturbations but only depends on how long control is available. Thus, the controller works precisely, forcing the spacecraft to follow the reference trajectory.

Figures 5.2 and 5.4 show the control histories of the simulations, each of which include four plots, the first three represent the control input required along the *R*, *S* and *W* directions, and the forth plot represents the magnitude of the resulting control acceleration vector. The maximum control acceleration required for maintain Sun-synchronous orbits comes out to around 1.5×10^{-6} km/sec^2, which for a spacecraft of mass 500 kg means that a maximum control thrust of 0.75 N is required (using $F = ma$). Current electric propulsion technology offers a wide variety of hardware that can produce such thrust levels, some of which include Hall thrusters designed by the Busek, Co. and ion thrusters developed by NASA and Aerojet (see Section 2.2).

The long term simulations of Orbit A show a repeating trend about every 14 days. This happens because the ascending node of the orbit measured with respect to the rotating frame increases by about 180 deg every 14 days due to the Moon's rotation. This makes the orbit plane orientation of the spacecraft to repeat every 14 days causing it to pass over the same lunar surface again and hence resulting in it being affected by the same lunar gravitational potential (since Ω and Ω+180 deg correspond to the same orbit plane).

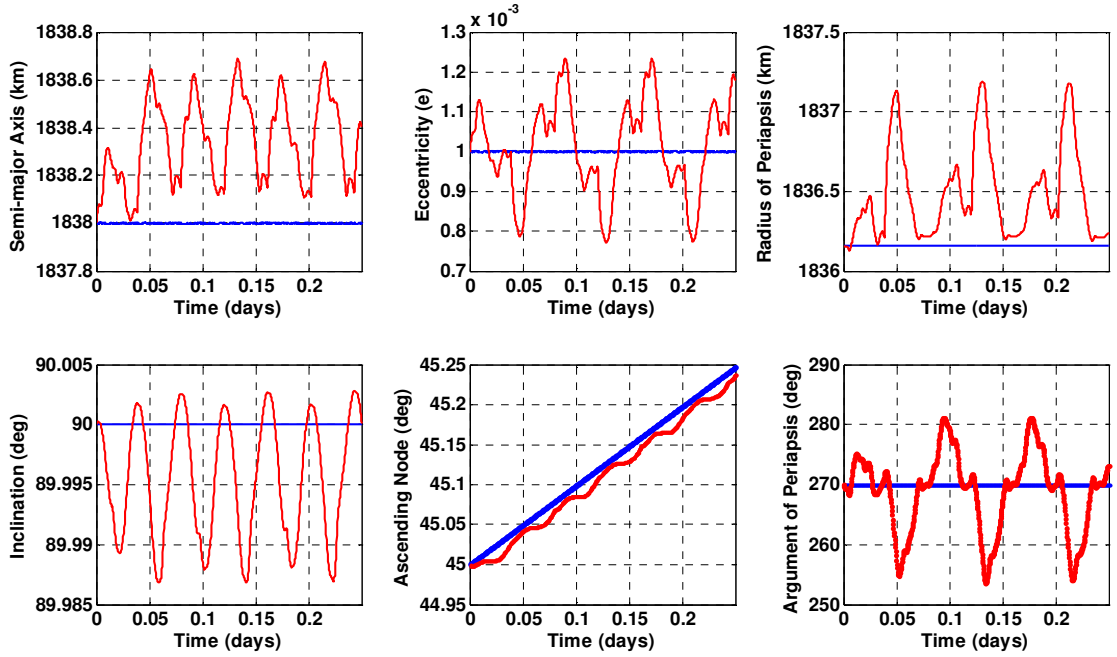

Figure 5.1 Controlled Sun-Synchronous Orbit A (Short-Term)

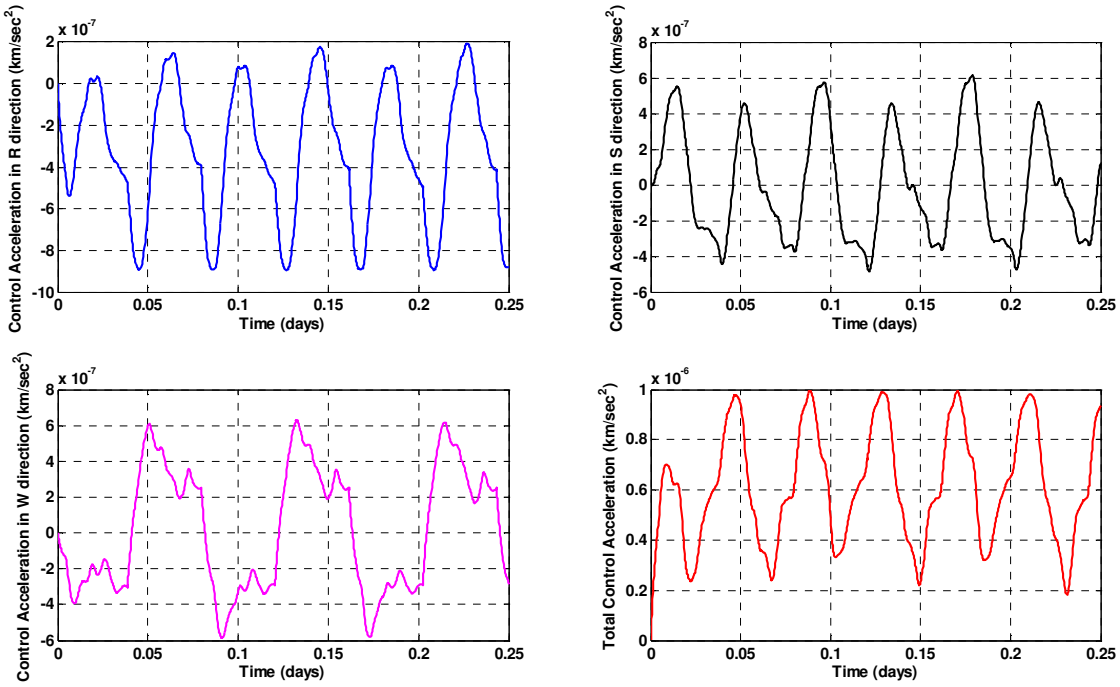

Figure 5.2 Control History for Sun-Synchronous Orbit A (Short-Term)

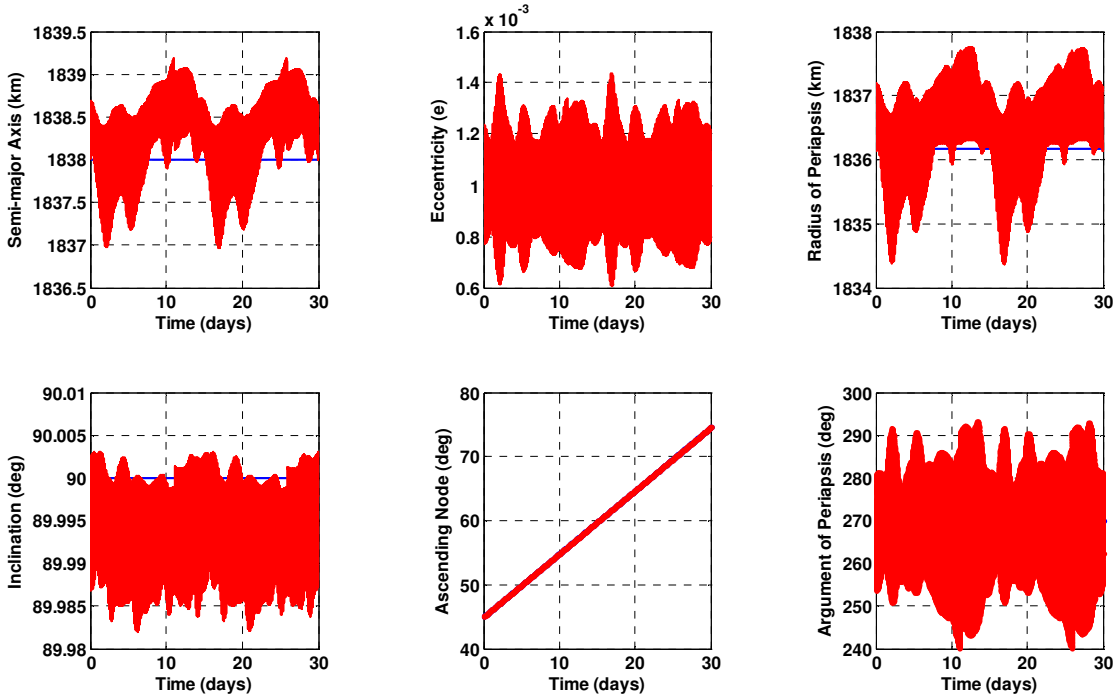

Figure 5.3 Controlled Sun-Synchronous Orbit A (Long-Term)

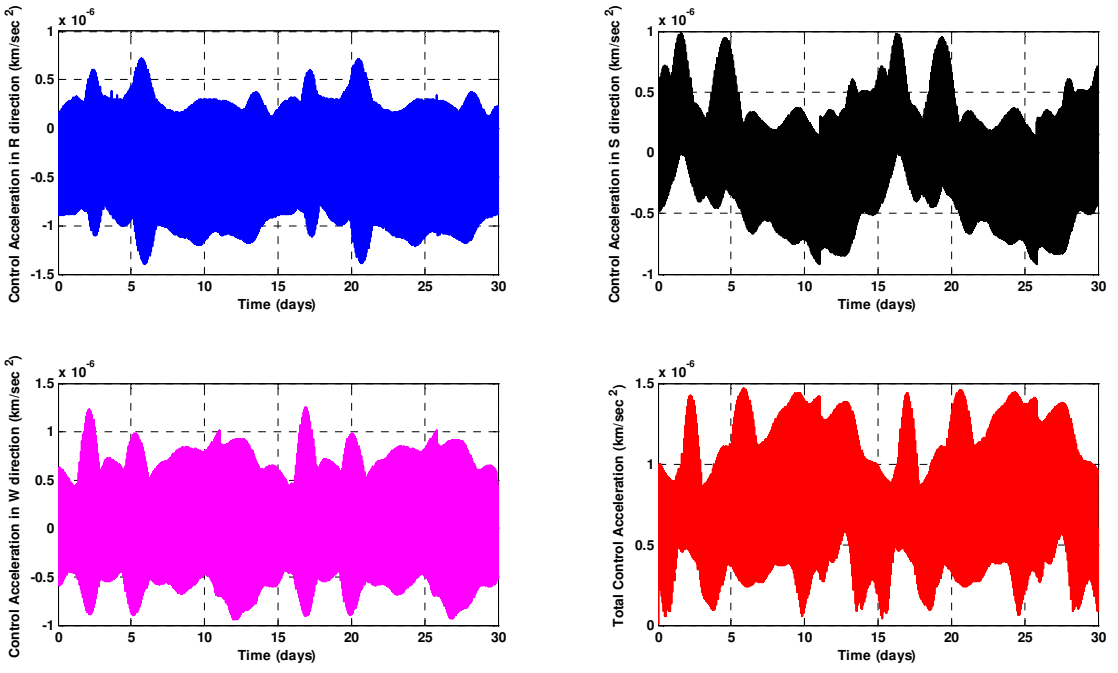

Figure 5.4 Control History for Sun-Synchronous Orbit A (Long-Term)

The second group of simulations performed involved maintaining the spacecraft in a high altitude geo-synchronous lunar orbit suitable for communication. The reference orbit for this case was considered to be an unperturbed propagation of Orbit C with its ascending node measured with respect to the inertial frame, increasing at a Sun-synchronous rate of about 13.17 deg per day such that the ascending node measured with respect to the rotating frame remains the same. The results obtained after performing short (few orbit revolutions) and long term (one month) simulations of the controlled spacecraft in Orbit C are presented in Figure 5.5 to 5.8. For these simulations the control gains are computed using the state error and control weights

$$Q_C = 5\times10^{-5}\cdot\begin{bmatrix} 1 & 0 & 0 & 0 & 0 & 0 \\ 0 & 1 & 0 & 0 & 0 & 0 \\ 0 & 0 & 1 & 0 & 0 & 0 \\ 0 & 0 & 0 & 1 & 0 & 0 \\ 0 & 0 & 0 & 0 & 1 & 0 \\ 0 & 0 & 0 & 0 & 0 & 1 \end{bmatrix}, \text{and } R_C = \begin{bmatrix} 50\times10^{9} & 0 & 0 \\ 0 & 25\times10^{9} & 0 \\ 0 & 0 & 10\times10^{9} \end{bmatrix}$$

The plots of inertial orbital elements show a maximum error of only about 1 deg in the geo-synchronous ascending node tracking and that in inclination is about 2.2 deg. These deviations, though somewhat large, are still acceptable and do not affect the coverage performance because of the orbit's high altitude. It can be seen that the radius of periapsis remains within a 20 km range from the reference offering a spacecraft operational lifetime that is not affected by orbit perturbations but only depends on how long control is available. Thus, the controller works precisely even for geo-synchronous orbits.

The control histories show that the maximum control acceleration required to maintain geo-synchronous orbits is around $3.7\times10^{-6}\ \text{km/sec}^2$, which is higher than that obtained for Sun-synchronous orbits. This is because the inertial orbit plane rotation required for geo-synchronous orbit is much higher than that for Sun-synchronous orbits. Thus, for a spacecraft of mass 500 kg, this leads to a maximum control thrust of 1.85 N. Though being quite high, these thrust levels can still be produced by the currently

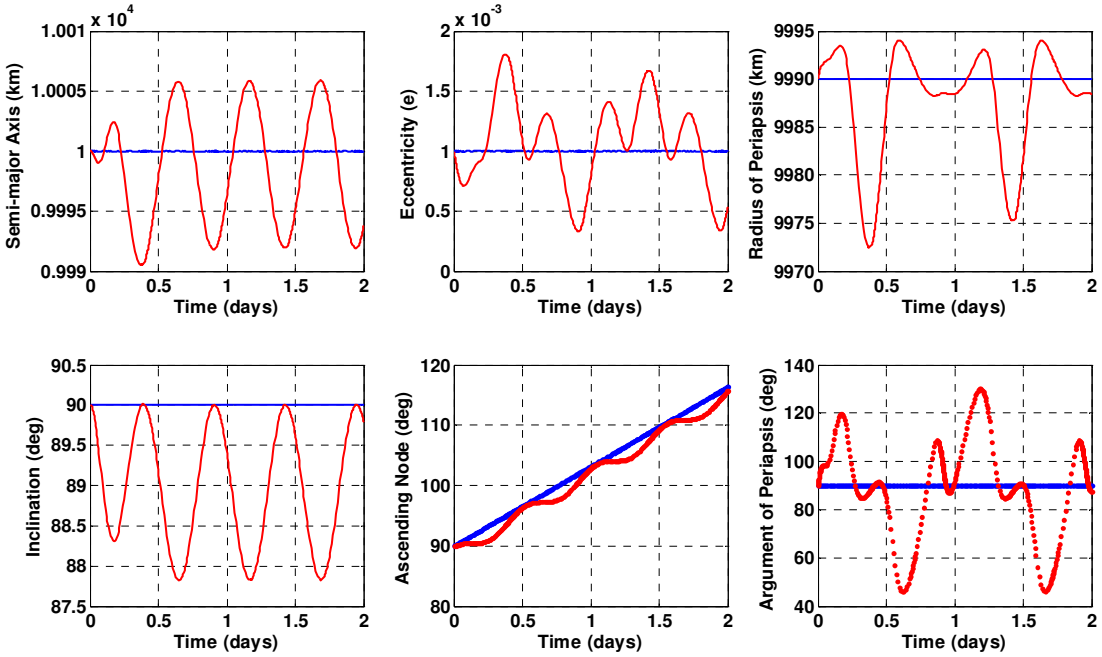

Figure 5.5 Controlled Geo-Synchronous Orbit C (Short-Term)

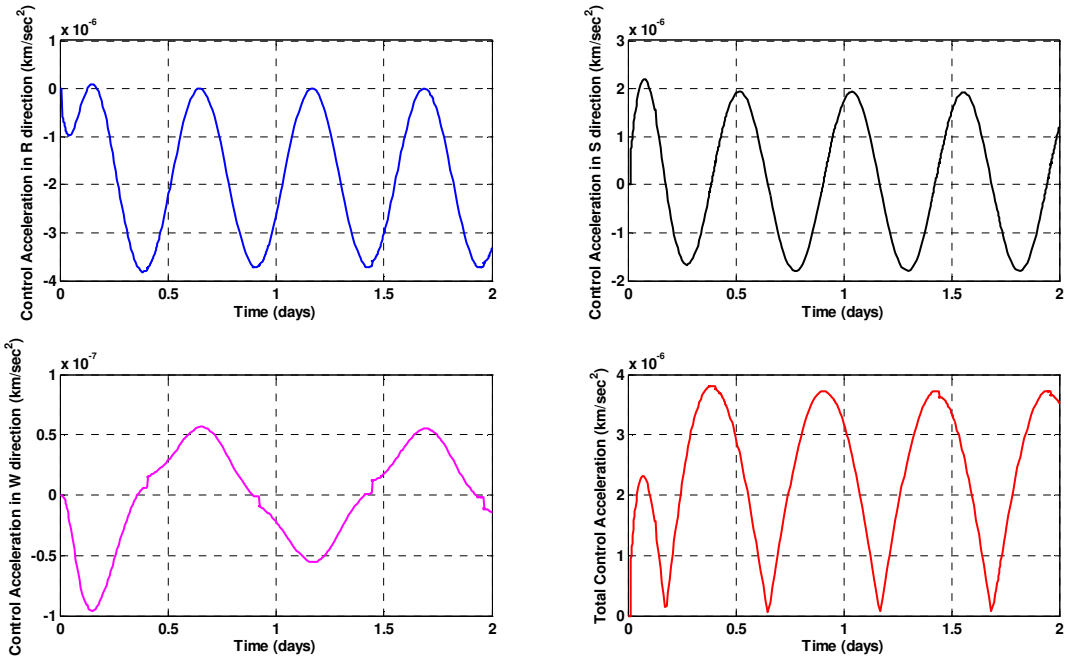

Figure 5.6 Control History for Geo-Synchronous Orbit C (Short-Term)

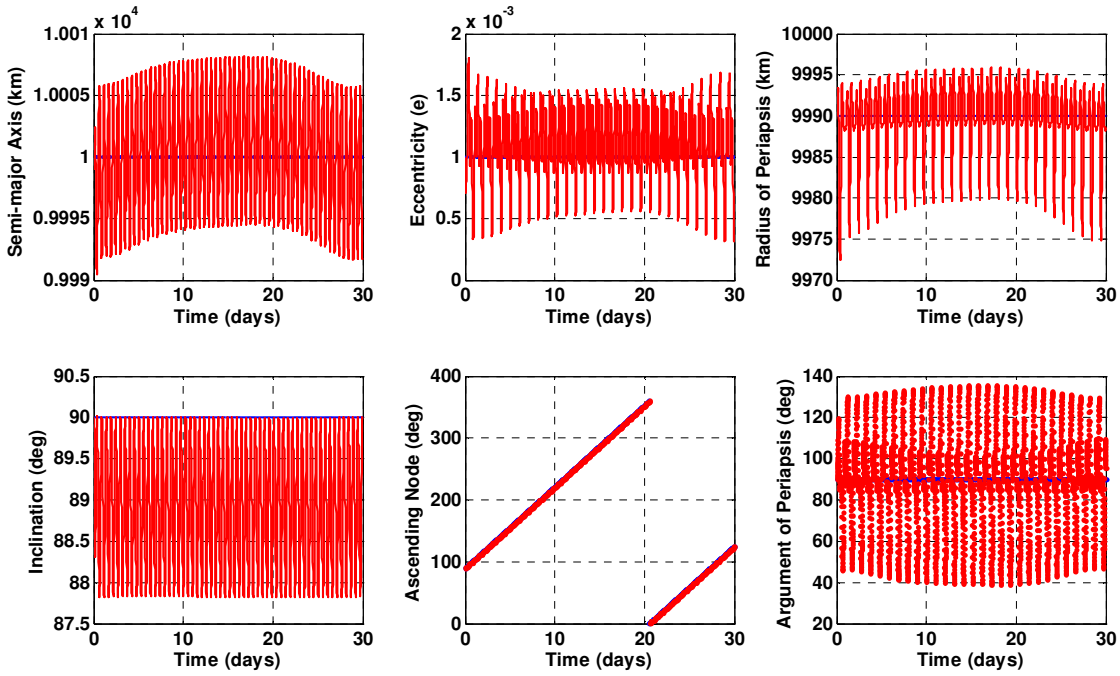

Figure 5.7 Controlled Geo-Synchronous Orbit C (Long-Term)

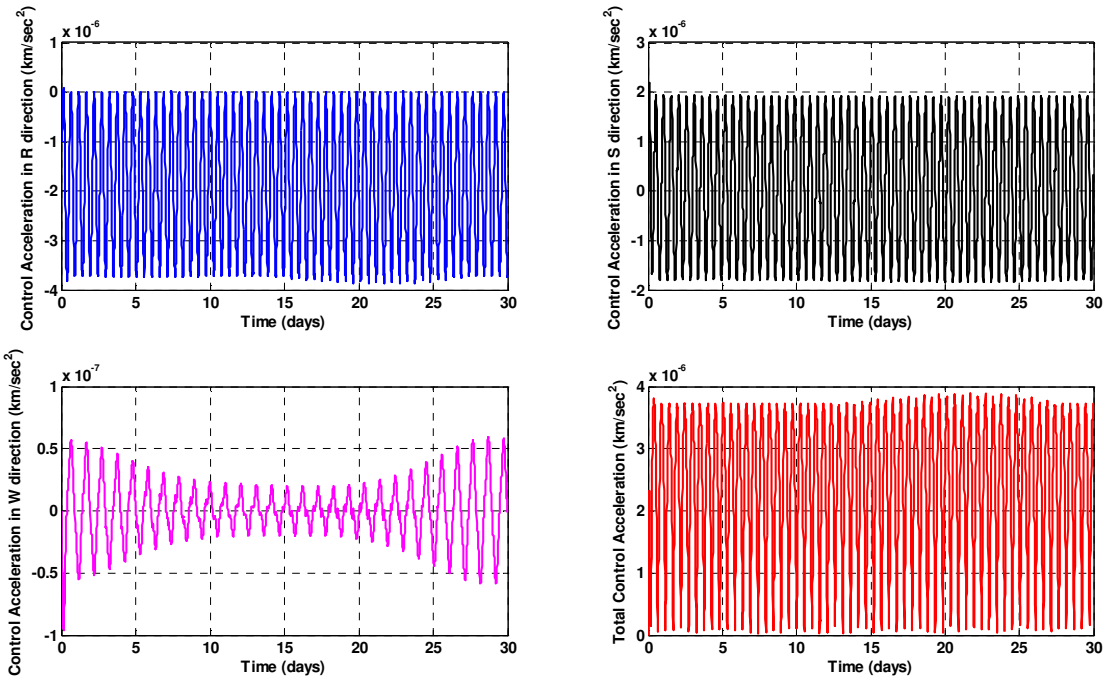

Figure 5.8 Control History for Geo-Synchronous Orbit C (Long-Term)

available electric propulsion hardware, such as the NASA's 457-M Hall thruster that uses krypton propellant and is capable of producing thrust levels up to 2.5 N. A string system of other thrusters designed by NASA, Busek, Co. and Aerojet, like HiPEP and NEXT (see Section 2.2) can also be used to obtain the high thrust values. A spacecraft can also use multiple low-thrust engines oriented in different directions, to obtain an overall higher range of continuous but varying control thrust vectors.

Unlike simulations of Orbit A, the long term simulations of Orbit C show no repeating trend every 14 days. This is because the ascending node of the orbit measured with respect to the rotating frame remains fixed due to the geo-synchronous inertial rotation. Thus, the orbit plane is always perpendicular to the Earth-Moon line and the spacecraft passes over nearly the same lunar surface in every orbit revolution.

A close look at all the short time control histories show that small unnoticeable variations in the repeating trajectory occur, when the spacecraft passes through areas where the coordinate x, y, or z is near zero, where a change in the choice of $A(X)$ was used to avoid infinite control forces. The use of different $A(X)$ matrices with constant weight matrices Q and R causes these variations. The areas correspond to the Moon's equatorial plane (where it is physically impossible to control the ascending node) and poles (where it is physically impossible to control the inclination).

5.2. CLOSED-FORM SOLUTION

While performing stability checks for the control law, an interesting observation is made. It is seen that real parts of the closed loop eigenvalues $E = EIG\ (A-B*K)$ are not just negative but they also remain nearly constant throughout the integration time. Intrigued by this behavior, all the elements of the control gain matrix, K were recorded for the integration time. It was found that the off-diagonal elements of the K matrix are not dominant and the dominant diagonal elements of the matrix are almost constant for the integration time. So, it turns out that by approximating the control gains, a closed-form solution that provides an analytic expression for the control law, can be found for this problem. For Orbit A, the constant control gain matrix turns out to be

$$K_A = \begin{bmatrix} 2.47\times10^{-6} & 0 & 0 & 0.002225 & 0 & 0 \\ 0 & 2.47\times10^{-6} & 0 & 0 & 0.002225 & 0 \\ 0 & 0 & 2.47\times10^{-6} & 0 & 0 & 0.002225 \end{bmatrix}.$$

For Orbit C, the constant gain matrix is given by

$$K_C = \begin{bmatrix} 2.6\times10^{-8} & 0 & 0 & 0.00025 & 0 & 0 \\ 0 & 2.6\times10^{-8} & 0 & 0 & 0.00028 & 0 \\ 0 & 0 & 2.6\times10^{-8} & 0 & 0 & 0.00036 \end{bmatrix}$$

The use of a constant gain for computing the control acceleration eliminates the online computations required for solving the Riccati equation at each time step. It also eliminates the need for changing the choice of *A(X)* matrix for time periods when the x, y or z coordinates are near zero. This makes the implementation of the controller very feasible, simple and easy. The control can then be straightforwardly computed using $\bar{u}_c = -K[X - X_{ref}]$, with controlled spacecraft dynamics given by

$$\ddot{\bar{r}}_{mo} = -\frac{\mu_e}{r_{eo}^{\ 3}}\bar{r}_{eo} - \frac{\mu_s}{r_{so}^{\ 3}}\bar{r}_{so} + \bar{\nabla}U_m + \bar{a}_{SRP} + \frac{\mu_e}{r_{em}^{\ 3}}\bar{r}_{em} + \frac{\mu_s}{r_{sm}^{\ 3}}\bar{r}_{sm} + \bar{u}_c$$

Figures 5.9 through 5.16 show the change in the inertial classical orbital elements and the required control accelerations of the spacecraft with respect to time, obtained after using a constant gain to compute control for short and long term simulations. They demonstrate the effectiveness of the closed-form solution since the orbits are precisely controlled. All these plots are very similar to the results obtained from the simulations in which the SDRE equation is solved at every time step to compute control (Figures 5.1 through 5.8).

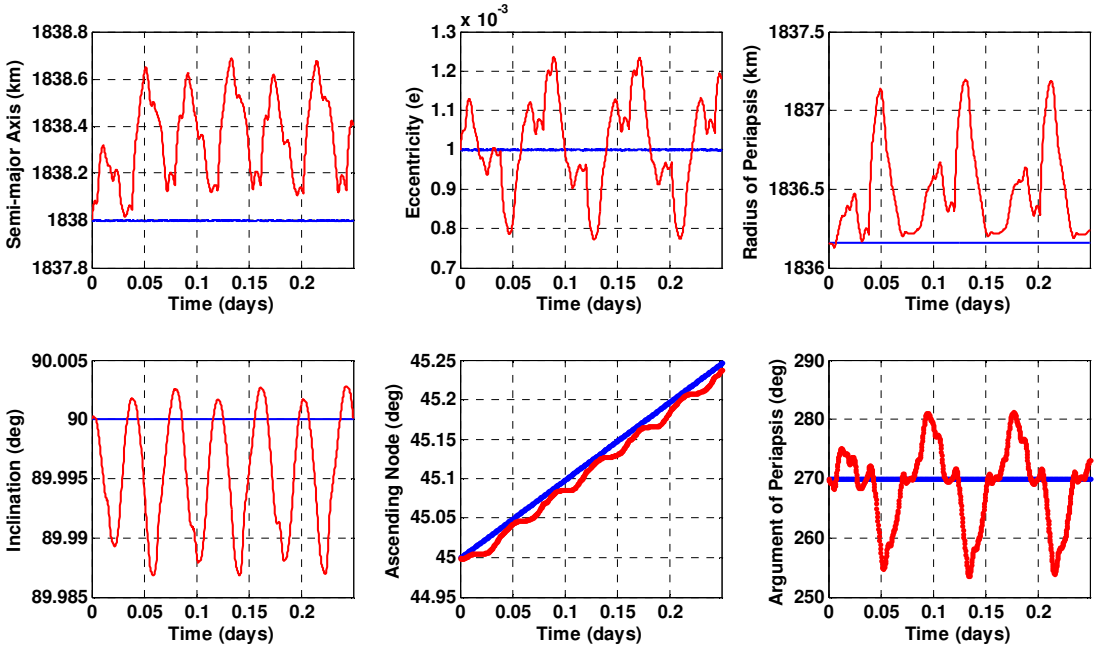

Figure 5.9 Constant Gain Controlled Sun-Synchronous Orbit A (Short-Term)

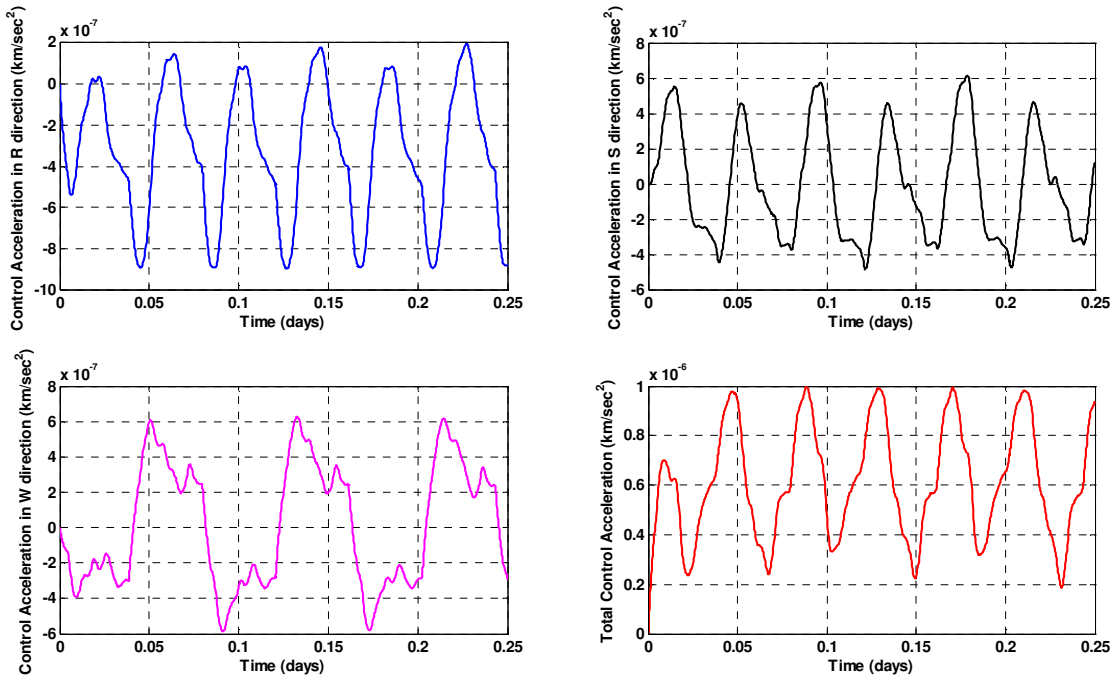

Figure 5.10 Constant Gain Control History for Sun-Synchronous Orbit A (Short-Term)

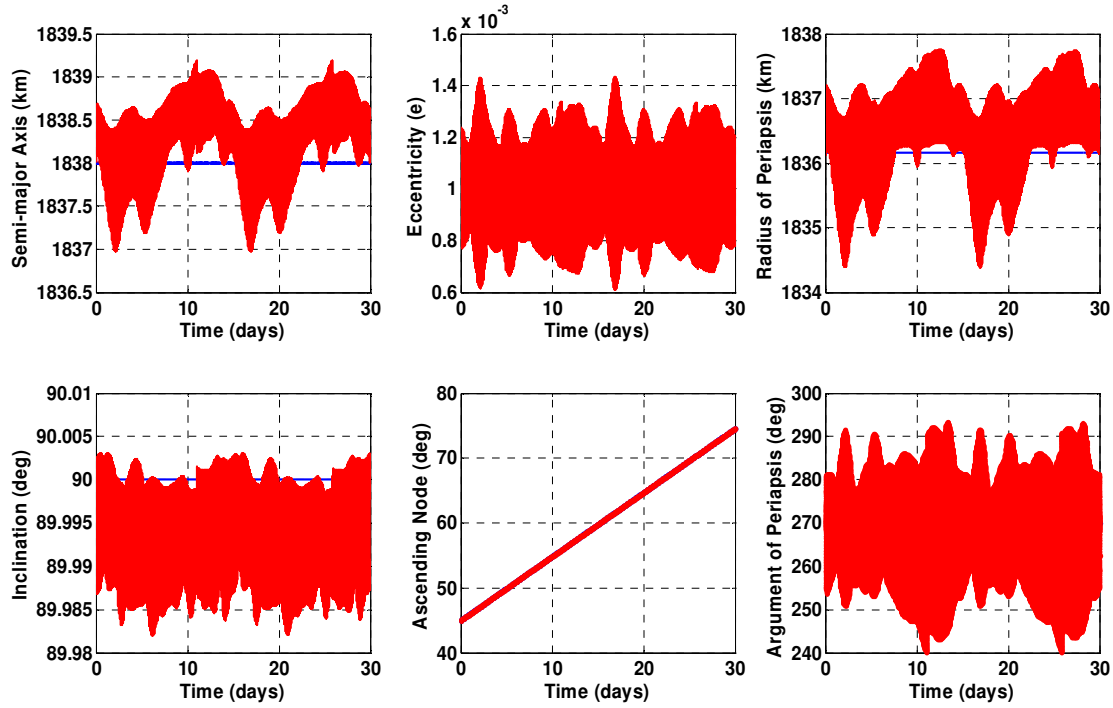

Figure 5.11 Constant Gain Controlled Sun-Synchronous Orbit A (Long-Term)

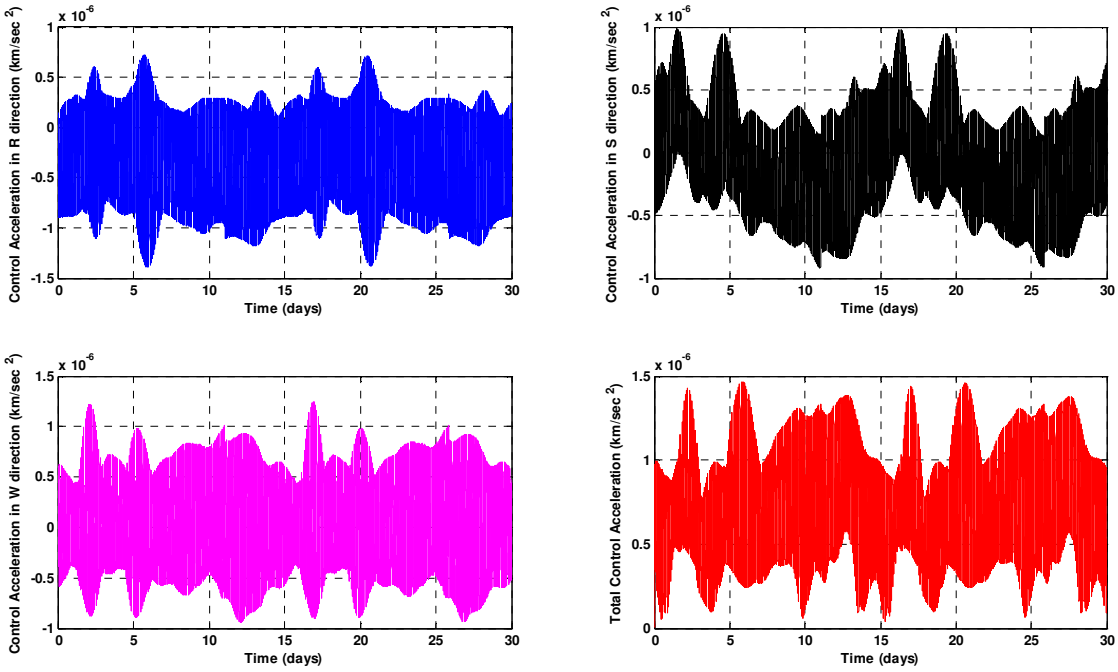

Figure 5.12 Constant Gain Control History for Sun-Synchronous Orbit A (Long-Term)

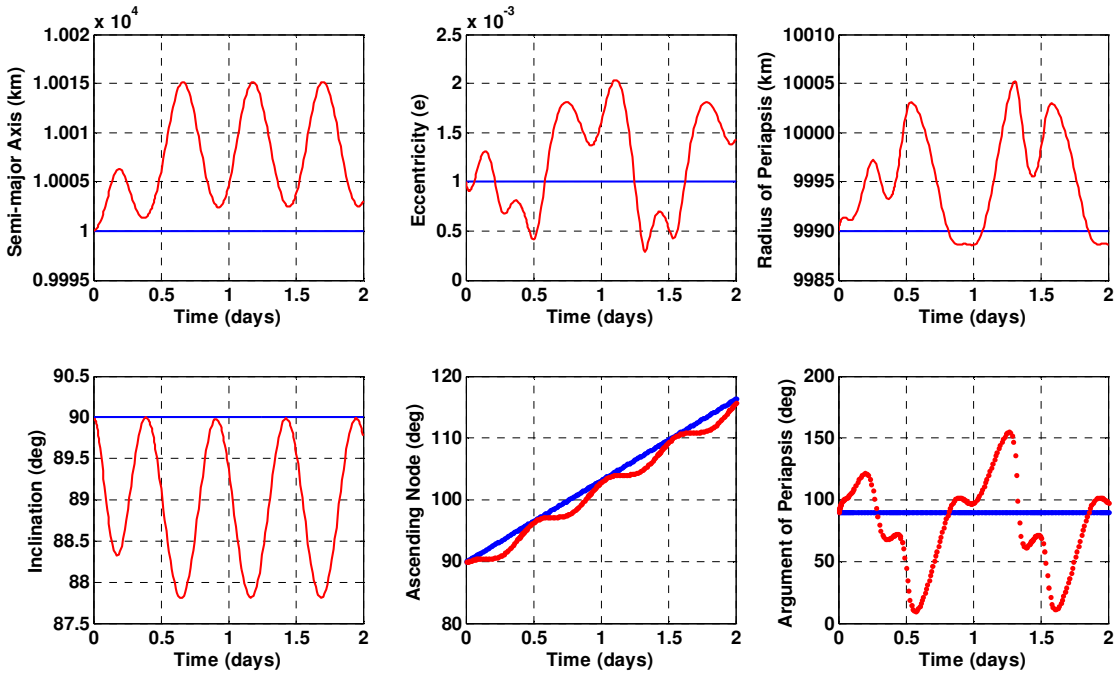

Figure 5.13 Constant Gain Controlled Geo-Synchronous Orbit C (Short-Term)

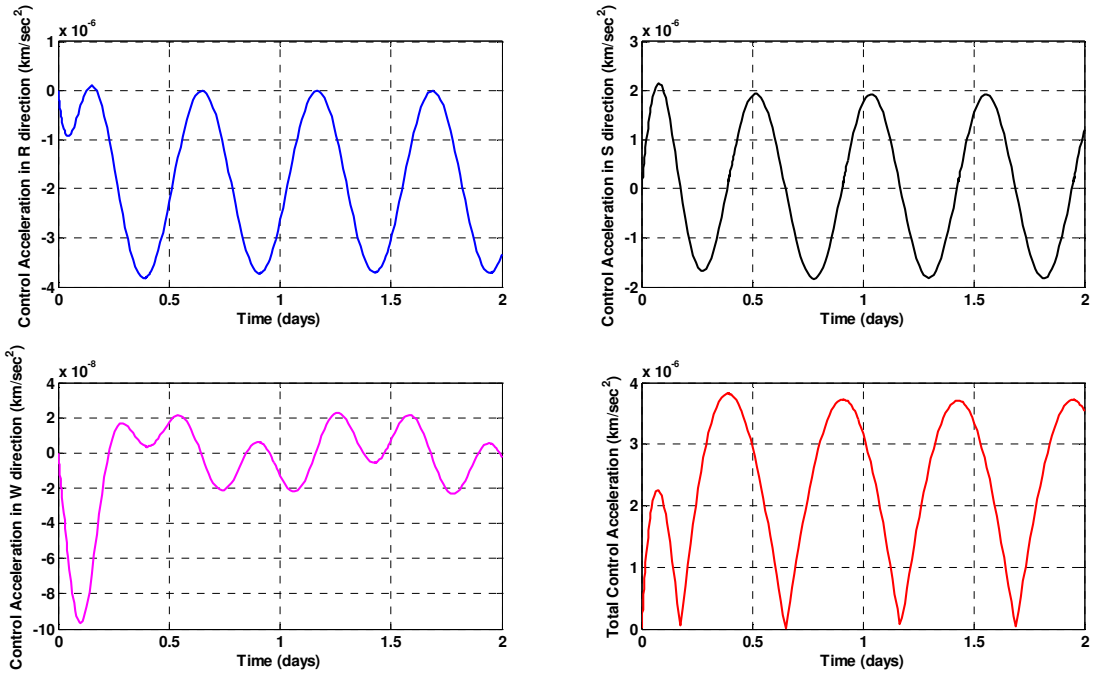

Figure 5.14 Constant Gain Control History for Geo-Synchronous Orbit C (Short-Term)

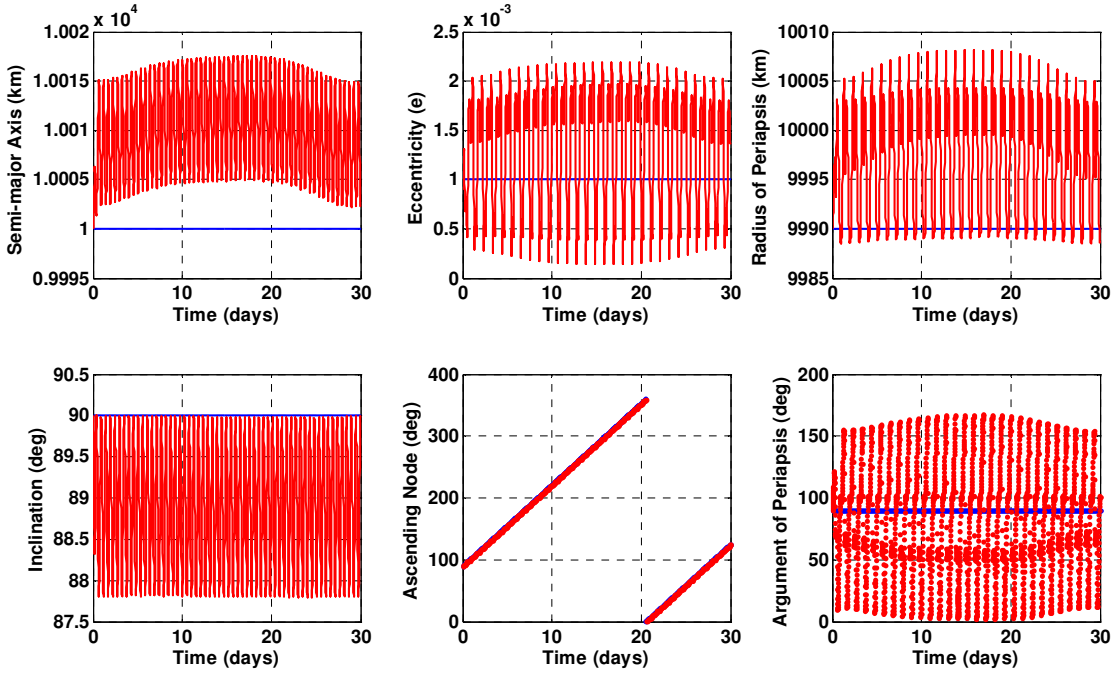

Figure 5.15 Constant Gain Controlled Geo-Synchronous Orbit C (Long-Term)

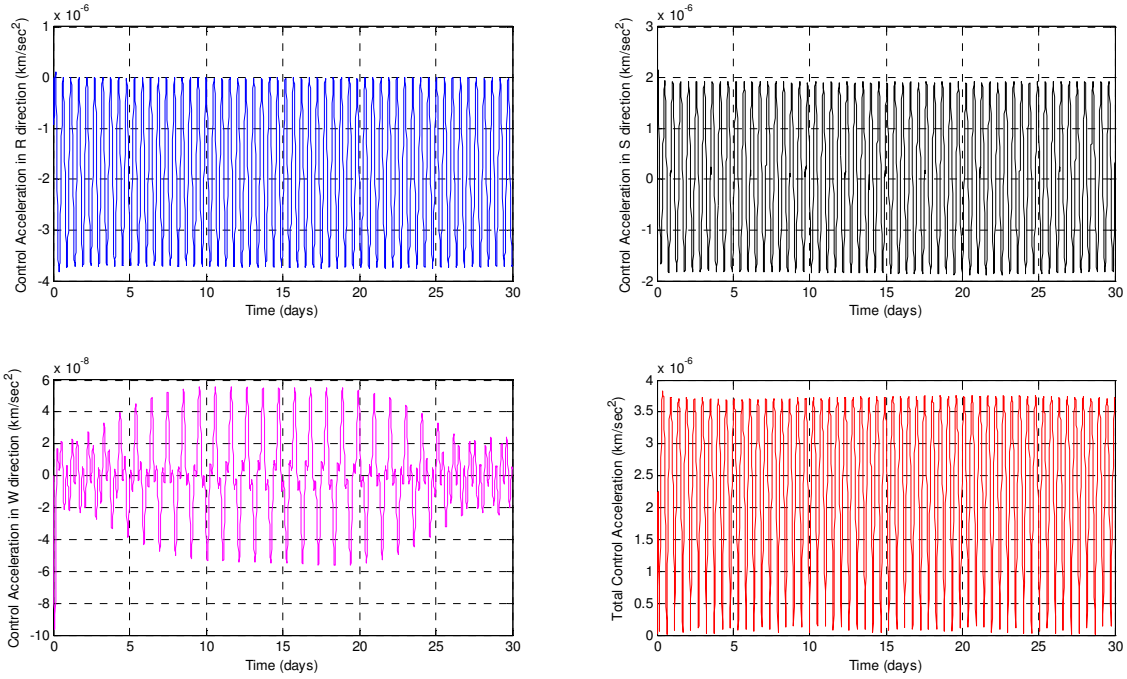

Figure 5.16 Constant Gain Control History for Geo-Synchronous Orbit C (Long-Term)

6. CONCLUSIONS AND FUTURE WORK

The impact of using electric propulsion on the search space of feasible and useful orbits for future lunar missions was studied and demonstrated successfully. At first, the requirements for future lunar mapping and communications were studied, and possible options to meet them were investigated. Based on coverage analysis, a new option was proposed, to provide a better communications architecture than those previously recommended in the open literature. This proposed architecture is a constellation of three satellites in high altitude, circular and polar geo-synchronous orbit that is always facing the Earth. It provides near global coverage and requires only three satellites, which can be placed in orbit with a single rocket launch instead of the four satellites and dual rocket launches required while using inclined frozen orbit constellations. Low altitude, polar, circular, Sun-synchronous orbits were found to be the most desired option to meet future lunar mapping needs. However, it was observed that these high performance options for lunar mapping and communication require a continuous orbit plane rotation and orbit stationkeeping to provide reliable and consistent performance, thus needing continuous control inputs from an onboard propulsion system. The feasibility of using electric propulsion for providing such control was then determined.

After modeling the nonlinear dynamics of the spacecraft which incorporates perturbations from the nonspherical Moon, Earth and Sun, a robust suboptimal controller based on the state dependent algebraic Riccati equation (SDRE) approach was formulated to control lunar orbits. Using this controller, a highly accurate and precise control of the spacecraft orbiting the Moon in a near-polar, near-circular Sun-synchronous orbit (suitable for mapping) and geo-synchronous orbit (suitable for communications) was achieved. A closed-form solution for the control law was obtained by approximating the control gains and was found to give similar results as that from using the SDRE technique. This closed-form solution provides an analytic expression for the control law and eliminates the need for solving the Riccati equation at each time step, significantly reducing the required online computations and making the implementation of the controller very simple and easy.

Numerical results demonstrated that the proposed method of spacecraft control yields low control accelerations which can be provided by currently available electric propulsion hardware. This results in the conclusions that the use of electric propulsion makes more feasible and performance-enhancing options available for lunar missions, rather than just the traditional frozen orbits.

The results obtained from this research seem promising, but a significant amount of additional work is still needed to determine and assess the viability of electric propulsion for use in lunar orbit control. A trade study should to be performed and the most effective choices of mapping and communication architectures controllable by electric propulsion should be formally compared with architectures that incorporate an impulsive control strategy. The results obtained from the SDRE-based control strategy presented in this thesis need to be compared with other optimal control methods, to evaluate its performance and to justify its application. The impact of scheduling the control and state error weights on the control levels need to be studied, to determine if more effective solutions can be provided using SDRE-based controllers. The possibility of selective control of orbital elements also needs to be considered to obtain better and more feasible control trajectories. The impact of a varying and continuous thrust vector on the attitude control of lunar orbiters should also be studied. In this thesis, the use of electric propulsion for lunar orbit control was concluded to be feasible by showing that the maximum levels of control accelerations obtained after simulations of various orbits can be provided by current electric propulsion hardware. However, the capabilities of current hardware to provide the control trajectory i.e. variations in the control levels with time, also need to be investigated.

BIBLIOGRAPHY

1. http://en.wikipedia.org/wiki/Vision_for_Space_Exploration, Vision for Space Exploration, Nov. 2008.

2. http://nssdc.gsfc.nasa.gov/planetary/lunar. Lunar Exploration at the National Space Science Data Center, Nov. 2008.

3. http://www.nasa.gov/worldbook/moon_worldbook.html. World Book at NASA-Moon, Nov. 2008.

4. H. Spencer, H., Caroll, K. A., Arkani-Hamed, J., Zee, R. E., "Lunette: Lunar Gravity Mapping With A Nanosatellite," 13th CASI Conference on Astronautics, Montreal, Canada, April 2006.

5. Meyer, K.W., Buglia J.J., Desai, P.N., "Lifetimes of Lunar Satellite Orbits," NASA Technical Paper 3394, March 1994.

6. http://science.nasa.gov/headlines/y2006/06nov_loworbit.htm. Bizarre Lunar Orbits, Jan. 2009.

7. http://science.nasa.gov/headlines/y2006/30nov_highorbit.htm. A New Paradigm for Lunar Orbits, Jan. 2009.

8. http://news.nationalgeographic.com/news/2006/12/061204-moon-base.html. Moon Base Announced by NASA, Dec. 2008.

9. http://www.space.com/missionlaunches/moon_southpole_030604.html. Lunar South Pole Landing Sites Studied, Feb. 2009.

10. Nozette, S., et al, "The Clementine Mission to the Moon: Scientific Overview", *Science*, Vol. 266, 1835-1862 (1994).

11. Lozier, D., Galal, K., Folta, D., Beckman, M., "Lunar Prospector Mission Design and Trajectory Support", AAS 98-323, pp. 297–311 (1998).

12. http://www.space.com/businesstechnology/080430-tw-lunar-communication-post.html. Lunar Explorers Will Need MoonSat System, Jan. 2009.

13. Boain, Ronald J., "A-B-C's of Sun-Synchronous Orbit Mission Design," AAS/AIAA Space Flight Mechanics Conference, 2005.

14. Takano, Y., Takizawa, Y., Sasaki, S., "The SELENE project and Japanese Future Lunar Exploration," *Acta Astronautica* 57 (2005) 112 – 115, published by Elsevier Ltd.

15. Neuner, G. E., "Lunar Communication Satellite Systems," Master's Thesis, University of California, Los Angeles, January 1963.

16. Farquhar, R. W., "Lunar Communications with Libration-Point Satellites," AIAA *Journal of Spacecraft and Rockets*, Vol. 4, No. 10, Oct. 1967.

17. Carpenter, J., Folta, D., Moreau, M., and Quinn, D., "Libration Point Navigation Concepts Supporting the Vision for Space Exploration," AIAA 2004-4747, AIAA/AAS Astrodynamics Specialist Conference, Providence, Rhode Island, August 16-19, 2004.

18. Grebow, D., Ozimek, M., Howell, K., and Folta, D., "Multi-Body Orbit Architectures for Lunar South Pole Coverage," AAS 06-179, AAS/AIAA Space Flight Mechanics Conference, Tampa, Florida, January 22-26, 2006.

19. Hill, K., Parker, J., Born, G.H., Loz, M.W., "Low Cost Lunar Communication and Navigation," Project Geryon, Colorado Center for Astrodynamics Research (CCAR), Nov. 2006.

20. Ely, T., Lieb, E., "Constellations of Elliptical Inclined Lunar Orbits Providing Polar and Global Coverage," AAS 05-343 paper, AAS/AIAA Astrodynamics Specialist Conference, Lake Tahoe, California, August 2005.

21. Park, Sang-Young and Junkins, John L., "Orbital Mission Analysis for a Lunar Mapping Satellite," *The Journal of the Astronautical Sciences*, Vol. 43, No.2, pp.207-217 (1995).

22. Elipe A., and Lara, M., "Frozen Orbits about the Moon", *Journal of Guidance, Control, and Dynamics*, Vol26, No.2, March-April 2003.

23. Ramanan, R.V. and Adimurthy, V., "An Analysis of Near-Circular Lunar Mapping Orbits," *Journal of Earth Syst. Sciences*, Dec. 2005, pp. 619-626.

24. Folta, D. and Quinn, D., "Lunar Frozen Orbits," AIAA/AAS Astrodynamics Specialist Conference and Exhibit, 21 - 24 August 2006, Keystone, Colorado.

25. Lara, M., Russell, R. P., "Repeat Ground Track Lunar Orbits in the Full-Potential Plus Third-Body Problem," AIAA 2006-6750, AIAA/AAS Astrodynamics Specialist Conference and Exhibit, 21 - 24 August 2006, Keystone, Colorado.

26. Space Communication Architecture Working Group (SCAWG): NASA Space Communication and Navigation Architecture Recommendations for 2005-2030. Final Report, May 15, 2006.

27. Grebow, D., Ozimek, M., Howell, K., and Folta, D., "Design of Optimal Low Thrust Pole-Sitter Missions," AAS 09-148, AIAA/AAS Space Flight Mechanics Conference, Savannah, GA, Feb 2009.

28. Schier, J. "NASA's Lunar Space Communication and Navigation Architecture," AIAA 092407.

29. Hamera, K., Mosher, T., Gefreh, M., Paul, R., Slavkin, L., Trojan, J., "An Evolvable Lunar Communication and Navigation Constellation Concept," AIAA-2008-5480, 26th International Communications Satellite Systems Conference, San Diego, California, June 10-12, 2008.

30. Schmidt, Wayne M. and Andrews, John C., "Interests in Electric Propulsion," U.S. Air Force Astronautics Laboratory, California 1988-005.

31. Losa, D., Lovera, M., Drai, R., Dargent, T. and Amalric, J., "Electric Station Keeping of Geostationary Satellites: a Differential Inclusion Approach," 44th IEEE Conference on Decision and Control, and the European Control Conference 2005 Spain.

32. Oh, D. Y., Landau, D., Randolph, T., Timmerman, P., Chase, J., Sims, J., "Analysis of System Margins on Deep Space Missions Utilizing Solar Electric Propulsion," 44th AIAA/ASME/SAE/ASEE Joint Propulsion Conference & Exhibit, 21 - 23 July 2008, Hartford, CT.

33. Groot, W.A. de, "Propulsion Options for Primary Thrust and Attitude Control of Microspacecraft," COSPAR Colloquium on Scientific Microsatellites cosponsored by the Committee on Space Research, International Academy of Astronautics, and the National Science Council (NSC) Tainan, Taiwan, ROC, December 14–17, 1997.

34. Patterson, M. J. and Benson, S. W., "NEXT Ion Propulsion System Development Status and Capabilities," NASA/TM-2008-214988, Technical Memorandum, NASA Glenn Research Center, Jan. 2008.

35. Edwards, C. H. and Gabriel, S.B., "Ion Thrusters for Orbit/Attitude Control of Large Flexible Spacecraft," IEEE Colloquium on High Accuracy Platform Control in Space, 14 Jun 1993, London, UK.

36. http://dawn.jpl.nasa.gov, DAWN, Feb. 2009.

37. Wilson, Fred C., "Recent Advances in Satellite Propulsion and Associated Mission Benefits," AIAA International Communications Satellite System Conference, 2006.

38. Dunning, J. W. Jr., Hamley, J. A., Jankovsky, R. S. and Oleson, S. R., "An Overview of Electric Propulsion Activities at NASA," 40th AIAA/ASME/SAE/ ASEE Joint Propulsion Conference and Exhibit 11-14 July 2004, Fort Lauderdale, Florida.

39. Jacobson, D. T. and Manzella, D. H., "NASA's 2004 Hall Thruster Program," 40th AIAA/ASME/SAE/ASEE Joint Propulsion Conference and Exhibit 11-14 July 2004, Fort Lauderdale, Florida.

40. Milligan, D., Gestal, D. and Camino, O., "SMART-1 Electric Propulsion: An Operational Perspective," AIAA 2006-5767, the 9th International Conference on Space Operations, Rome, June 19 –23, 2006.

41. Jacobson, D. T. and Manzella, D. H., "50 kW Class Krypton Hall Thruster Performance," 39th AIAA/ASME/SAE/ASEE Joint Propulsion Conference and Exhibit, 20-23 July 2003, Huntsville, Alabama, *AIAA Journal*, 2003-4550.

42. Saccoccia, G., "Overview of European Electric Propulsion Activities," AIAA 2001-3228, 37th AIAA/ ASME/SAE/ASEE Joint Propulsion Conference and Exhibit, 8-11 July 2001, Salt Lake City, Utah.

43. Cassady, R. J., Meckel, N. J., Hoskins, W. A., Myers, R. M., Oleson, S. R. and McGuire, M., "Pulsed Plasma Thruster Systems for Spacecraft Attitude Control." Proc. 10th AIAA/USU Conference on Small Satellites, 1996.

44. Foster, J. E., Haag, T., Patterson, M., Williams, G.J., Sovey, J. S., Carpenter, C., Kamhawi, H., Malone, S. and Elliot, F., "The High Power Electric Propulsion (HiPEP) Ion Thruster," AIAA–2004–3812, 40th AIAA/ASME/SAE/ASEE Joint Propulsion Conference and Exhibit, Florida, 2004.

45. http://www.aerojet.com/capabilities/spacecraft.php, Aerojet Capabilities: Spacecraft Propulsion, Feb. 2009.

46. http://www.fathom.com/course/21701743/session4.html, The Past and Future of Rocket Engine Propulsion: Part II-Electrothermal Systems, Feb. 2009.

47. http://www.nasa.gov/offices/oce/llis/0736.html, Arcjet Thruster Design Considerations for Satellites, Feb. 2009.

48. http://www.busek.com/downloads/HighPower.pdf, BUSEK Space Propulsion: High Power Hall Effect Thruster Systems, Feb. 2009.

49. http://www.dodsbir.net/SuccessStories/busek.htm, A DoD SBIR Success Story: Busek Company, Inc., Feb. 2009.

50. http://www.nasa.gov/centers/glenn/about/fs23grc.html, Glenn Research Center: Pulsed Plasma Thrusters, Feb. 2009.

51. http://en.wikipedia.org/wiki/VASIMR, Variable Specific Impulse Magnetoplasma Rocket on Wikipedia, Feb. 2009.

52. http://science.nasa.gov/newhome/headlines/prop06apr99_2.htm, Ion Propulsion: Over 50 Years in the Making, Feb. 2009.

53. Hunziker, Raul R., "Low-Thrust Station Keeping Guidance for a 24-Hour Satellite," *AIAA Journal,* Vol. 8, No. 7, 1970, pp. 1186-1192.

54. Peissinger, R., "Optimal Continuous Thrust Orbital Evasive Maneuvers from Geosynchronous Orbit," M.S. Thesis, Air Force Inst. Of Tech., Dec. 1986.

55. Widhalm, J. W. and Eide, S. A., "Optimal Continuous Thrust In-Plane Evasive Maneuvers," AIAA Aerospace Sciences Meeting, 26th, Reno, NV, Jan. 11-14, 1988.

56. Sidi, M., "A Novel Control-Guidance Law for Low Thrust Orbit," 31st Israel Annual Conference on Aviation and Astronautics pp. 81-88, 02/1990.

57. Kluever, C. A., "Maximum-Payload Transfers to Geosynchronous Orbit Using Arcjet Thrusters," *J. Spacecraft*, Vol. 34, No. 3.

58. Palutan, F., De Martino, D., Falzini, S., Melis, M., "Geostationary Station-Keeping by Ion Thrusters: Genetic Algorithms Optimization," *International Journal of Satellite Communications*, Vol. 14, No.1, pp. 1-9, 1996.

59. Oleson, Steven R., Myers, Roger M., Kluever, Craig A., "Advanced Propulsion for Geostationary Orbit Insertion and North-South Station Keeping," *Journal of Spacecraft and Rockets*, Vol. 34, No. 1, 1997.

60. Kluever, C. A., "Comet Rendezvous Mission Design Using Solar Electric Propulsion Spacecraft," *Journal of Spacecraft and Rockets*, Vol. 37, No. 5, September–October 2000.

61. Edelbaum, T. N., "Optimum Low Thrust Rendezvous and Station Keeping," *Journal of Spacecraft and Rockets*, Vol. 40, No. 6, pp. 960-965, 2003.

62. Losa, D., Lovera, M., Drai R., Dargent, T., Amalric, J., "Electric Station Keeping of Geostationary Satellites: a Differential Inclusion Approach," 44th IEEE Conference on Decision and Control, and the European Control Conference 2005 Seville, Spain, December 12-15, 2005.

63. Gomes, V.M., Prado, A. F. B. de A., and Kuga, H. K., "Orbital Maneuvers Using Low Thrust to Place a Satellite in a Constellation," Hindawi Publishing Corporation, *Mathematical Problems in Engineering*, Vol. 2007, Article ID 98532, October 2006.

64. Gurfil, P., "Nonlinear Feedback Control of Low Thrust Orbital Transfer in a Central Gravitational Field," *Acta Astronautica* 60 (2007) 631 – 648.

65. Oleson, Steven R., "Mission Advantages of Constant Power, Variable Isp Electrostatic Thrusters," AIAA 2000-3413, 36th AIAA/ASME/3AE/A3EE Joint Propulsion Conference & Exhibit July 16-19, 2000/Huntsville, AL.

66. Zhang, Z. and Li, J., "Orbit and Attitude Control of Spacecraft Formation Flying," *Appl. Math. Mech. Journal*, Vol. 29, No. 1, pp. 43–50, 2008.

67. Erdrm, E.B., "Analysis and Real-time Implementation of State-Dependent Riccati Equation Controlled Systems," PhD Thesis, University of Illinois at Urbana-Champaign, 2001.

68. Terui, F., "Position and Attitude Control of a Spacecraft by Sliding Mode Control," *Proceedings of the American Control Conference*, Philadelphia, PA, June, 1998.

69. Kim, Ki-Seok and Kim, Y., "Backstepping Control of Rigid Spacecraft Slew Maneuver," AIAA Guidance, Navigation, and Control Conference and Exhibit, August 2001 , Montreal, Canada.

70. Hwang, C. L., "Sliding Mode Control using Time-Varying Switching Gain and Boundary Layer for Electrohydraulic Position and Differential Pressure Control," *IEEE Proceedings*, Online No. 1 9960377, November I995

71. Cloutier, J.R., "State-Dependent Riccati Equation Techniques: An Overview," American Control Conference, Albuquerque, New Mexico, June 1997.

72. E. Bryson and Y. C. Ho, "*Applied Optimal Control,"* Hemisphere Publishing Co., New York, 1975.

73. Lewis, F. L. and Syrmos, V. L., "*Optimal Control,"* Wiley-IEEE, 1995.

74. Çimen, Tayfun, "State-Dependent Riccati Equation (SDRE) Control: A Survey," 17th World Congress , The International Federation of Automatic Control, Seoul, Korea, July 6-11, 2008.

75. Kluever, Craig A. and Oleson, Steven R., "Direct Approach for Computing Near-Optimal Low-Thrust Earth-Orbit Transfers," *Journal of Spacecraft and Rockets*, Vol. 35, No. 4, July–August 1998.

76. Harl, Nathan, "Low-Thrust Control of a Lunar Orbiter," Master's Thesis, Missouri University of Science and Technology, Rolla, Missouri, 2008.

77. Stansbery, D.T. and Cloutier, J.R., "Position and Attitude Control of a Spacecraft Using the State Dependent Riccati Equation Technique," *Proceedings of the American Control Conference*, Chicago, IL, June, 2000.

78. Luo, Wencheng and Chu, Yum-Chung, "Attitude Control Using the SDRE Technique," Seventh International Conference on Control, Automation, Robotics And Vision (ICARCV'O2), Dec 2002, Singapore.

79. Xin, M., Balakrishnan, S.N. and Stansbery, Donald T., "Spacecraft Position and Attitude Control with θ -*D* Technique," 42nd AIAA Aerospace Sciences Meeting and Exhibit, 5 - 8 January 2004, Reno, Nevada.

80. Bain, J. and Sunkel, J., "Autonomous Control for Subsonic Flight of X-38," paper AIAA-98-4567.

81. Barbieri, Enrique and Alba-Flores, Rocio, "A New Look at the Infinite-Horizon Linear-Quadratic Tracking Problem," 37th IEEE Conference on Decision & Control, Tampa, Florida USA December 1998.

82. Barbieri, Enrique and Alba-Flores, Rocio, "Real-Time Infinite Horizon Linear-Quadratic Tracking Controller for Vibration Quenching in Flexible Beams," 2006 IEEE Conference on Systems, Man, and Cybernetics October 8-11, 2006, Taipei, Taiwan.

83. Cloutier, J.R and Stansbery, D.T., "The Capabilities and Art of State-Dependent Riccati Equation-Based Design," American Control Conference, Anchorage, AK. May 8-10.2002.

84. Cloutier, J.R., D'Souza, C.N. and Mracek, C.P., "Nonlinear Regulation and Nonlinear Hinf Control Via the State-Dependent Riccati Equation Technique", *Proc. 1st International Conference On Nonlinear Problems in Aviation and Aerospace, AIAA Journal*, Reston, VA, Vol.1, 1996, pp. 117-123.

85. Cloutier, J.R and Zipfel, P.H., "Hypersonic Guidance via the State-Dependent Riccati Equation Control Method," IEEE International Conference on Control Applications, Kohala Coast-Island of Hawai'i, Hawai'i, USA August 22-27, 1999.

86. Escobal, Pedro Ramon, "*Methods of Astrodynamics*" J. Wiley & Sons, 1968.

87. Escobal, Pedro Ramon, "*Methods of Orbit Determination*" J. Wiley & Sons, 1965.

88. Vallado, David A., "*Fundamentals of Astrodynamics and Applications*" The Space Technology Library, Second Edition, 2004.

89. Curtis, Howard D., "*Orbital Mechanics for Engineering Students*," Elsevier, 2005.

90. Wertz, James R., "*Mission Geometry; Orbit and Constellation Design and Management,*" The Space Technology Library, 2001.

91. Jet Propulsion Laboratory, "Artificial Satellite Analysis Program (ASAP)," 1987.

92. http://pds-geosciences.wustl.edu/geodata/lp-l-rss-5-gravity-v1/lp_1001/sha/jgl165p1.sha, Lunar Prospector Spherical Harmonics and Gravity Models, Nov. 2008.

93. Aggarwal, S., Harl, N., Pernicka, H.J. and Balakrishnan, S.N., "Optimal Control of a Sun-synchronous Lunar Orbiter," AIAA Guidance, Navigation and Control Conference and Exhibit 2007, 20 - 23 August 2007, Hilton Head, South Carolina.

94. Harl, N. and Pernicka, H.J., "Low-Thrust Control of a Lunar Orbiter," 19th AAS/AIAA Space Flight Mechanics Meeting, Savannah, Georgia. February 8-12, 2009.

95. Mulville, D. R., "NASA's Lunar Robotic Architecture Study- Final Report" Technical Report, NASA/TM-2006-214067/VOL1.

VITA

Sunil Aggarwal was born in India on December 18, 1984 to Jag Jiwan Aggarwal and Asha Devi Aggarwal. He finished schooling from S.L.S.D.A.V. Public School in New Delhi, India in 2003. In December of 2006, he graduated with a Bachelor of Science degree in Aerospace Engineering with a 4.0 GPA, from the University of Missouri-Rolla (now Missouri University of Science and Technology). While at Missouri S&T, Sunil Aggarwal was actively involved in campus activities as a leader in aerospace design teams. He also received a Green belt in Six Sigma from Caterpillar, Inc. and served as the Vice President for the Missouri S&T chapter of Sigma Gamma Tau, Aerospace Engineering Honor Society. In May of 2009, he was awarded a Master of Science degree in Aerospace Engineering with highest honors by Missouri S&T. During his graduate studies, he was appointed as a teaching assistant at Missouri S&T for a year and he also gained work experience in aerospace systems at Rockwell Collins, Inc. located in Iowa. He is currently a member of Missouri S&T Chancellor's Leadership Academy Alumni, AIAA, Tau Beta Pi (Engineering Honor Society) and Sigma Gamma Tau.